Article

Automatic Generation of Local Vibrational Mode Parameters: From Small to Large Molecules and QM/MM Systems

Published as part of The Journal of Physical Chemistry virtual special issue "MQM 2022: The 10th Triennial Conference on Molecular Quantum Mechanics".

Renaldo T.MouraJr., Mateus Quintano, Juliana J. Antonio, Marek Freindorf, and Elfi Kraka*

Read Online

ACCESS | Metrics & More | Article Recommendations | Supporting Information

ABSTRACT: LModeAGen, a new protocol for the automatic determination of a nonredundant, complete set of local vibrational modes is reported, which is based on chemical graph concepts. Whereas local mode properties can be calculated for a selection of parameters targeting specific local modes of interest, a complete set of nonredundant local mode parameters is requested for the adiabatic connection scheme (ACS), relating each local vibrational mode with a normal mode counterpart, and for the decomposition of normal modes (CNM) in terms of local mode contributions, a unique way to analyze vibrational spectra. So far, nonredundant parameter sets have been generated manually following chemical intuition or from a set of redundant parameters in a trial-and-error fashion, which has hampered the study of larger systems with hundreds of parameters. LModeAGen

was successfully applied for a test set of 11 systems, ranging from small molecules to the large QM (>100 atoms) subsystem of carbomonoxy-neuroglobin protein, described with a hybrid QM/MM method. The ωB97X-D/aug-cc-pVDZ, M06L/def2-TZVP, and QM/MM ωB97X-D/6-31G(d,p)/AMBER model chemistries were adopted for the description of the molecules in the test set. Our new protocol is an important step forward for a routine ACS and CNM analysis of the vibrational spectra of complex and large systems with hundreds of atoms, providing new access to important encoded electronic structure information.
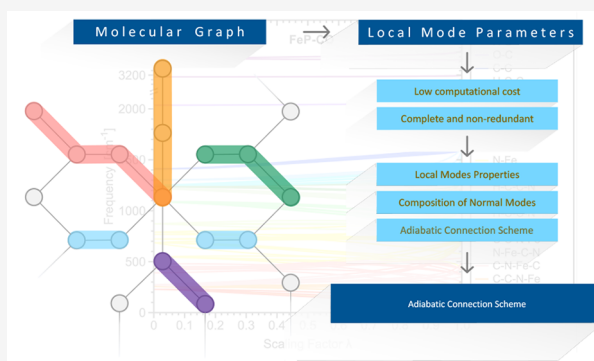
■ INTRODUCTION

Vibrational spectroscopy can reveal in-depth information on the electronic structure and bonding of chemical systems, where its applications and improvements have been of recent interest.[1−22] Nevertheless, the very nature of a normal vibrational mode (NVM) in polyatomic systems is generally marked by delocalization in the form of collective motion of fragments,[23] which makes it difficult to extract intrinsic bond properties and/or assigning contributions of a particular molecular fragment to a specific normal vibrational mode. The local vibrational mode (LVM) theory,[24,25] originally introduced by Konkoli and Cremer is a powerful tool to approach these complications by deriving local vibrations and associated local mode properties from NVMs, and to provide the foundation for the characterization of normal mode (CNM) procedure and the adiabatic connection scheme (ACS).[26−30]

ACS and CNM have led to comprehensive insights into vibrational spectra, as reported in the literature.[24,28−39] However, both require a complete nonredundant set of N_{vib} local vibrational modes. N_{vib} equals $3N - N_{tr}$, with the translational and rotational modes N_{tr} being 5 for a linear and 6

for a nonlinear molecule being composed of N atoms. It has to be noted that the selection of a chemically meaningful nonredundant set of local mode parameters is a nontrivial and formidable task, in particular for systems with high symmetry, for ring systems or larger complexes with N_{vib} in the hundreds. So far, the selection is often done manually, for example, starting with the inclusion of all bond lengths (N_B) and bond angles (N_A), and then adding dihedrals (N_D) and other parameters as needed, or starting from a set of redundant coordinates and eliminating parameters in a more or less trial and error procedure. This trial and error procedure works fine for smaller molecules, however can become a daunting, memory demanding and time-consuming task for larger systems. Previously, it was advised that N_B, N_A, and N_D should vary depending on whether the system is open-chain or
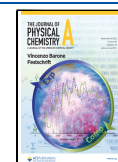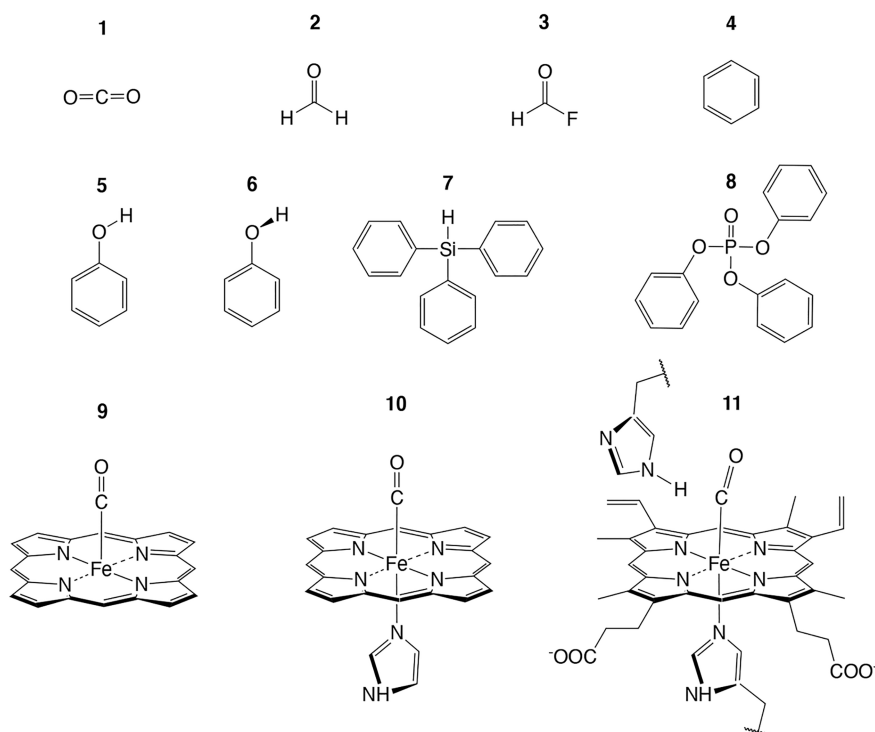
Figure 1. Schematic representations of the 11 test cases investigated in this work; examples **1**−**10**: single molecules of increasing size; example **11**: QM subsystem of an active site of carboxy-neuroglobin (NgbCO) in the ϵ tautomeric form of the distal histidine H64ϵ described with QM/MM.

cyclic,[31] yet the formulas that predict each of these numbers can still be generalized for systems containing multiple cycles. This generalization is discussed in detail in the next section in addition to cases containing linear subsystems.

Evidently, new ideas to facilitate the calculation of ACS and CNM are needed, which bolsters the importance of the new protocol discussed in this work. In this context, chemical graph theory[40] offers a convenient starting point for the generation of suited local mode parameters as a means to achieve (i) completeness, (ii) nonredundancy, and (iii) enhanced chemical meaning, which is fundamentally important for the interpretation of the vibrational spectra of molecules by means of CNM and ACS. Therefore, an efficient, consistent, and reliable protocol for obtaining the parameters that satisfy (i) − (iii) is expected to broaden the reach of applications involving systems of varying size and complexity. By considering a molecule or system of interest as a chemical graph, where the atoms are vertices and the intra- or intermolecular interactions are the edges, the local vibrational modes can be expressed as paths with two (bonds), three (angles), or four (dihedrals) distinct vertices and the corresponding local mode parameters can be obtained automatically via a proper interpretation of the connectivity matrix.

Figure 1 illustrates test examples **1**−**11**, which were adopted to challenge the capability of the new protocol reported in the present work for automatic generation of local vibrational mode parameters based on chemical graph concepts. Herein, the remarkable applicability of CNM/ACS to the decomposition of normal vibrational modes of intricate QM subsystems (test example **11**) is exemplified, where the extraction from the corresponding full QM/MM sets is carried out with the generalized subsystem vibrational analysis (GSVA) developed in our group.[41,42] We have also revisited

gas-phase systems that exhibit subtleties that are worth reevaluating (test examples **1**−**3**) or used to pose a conundrum to spectral analysis through LVM (test examples **4**−**10**),[35] relying solely on chemical intuition and specialized skills to arrive at the complete and nonredundant set of local vibrational modes.

■ METHODOLOGY

Local Vibrational Mode Theory. The mathematical apparatus of normal-mode analysis for a vibrating polyatomic molecule with N atoms is based upon the Wilson equation of vibrational spectroscopy[43−47]

$$\mathbf{F}^x \tilde{\mathbf{L}} = \mathbf{M} \tilde{\mathbf{L}} \Lambda \tag{1}$$

where $\mathbf{F}^x$ is the force constant matrix written in Cartesian coordinates x_i ($i = 1, ..., 3N$). $\mathbf{M}$ is the diagonal mass matrix comprising the atomic mass for each atom three times to account for the motion in the x, y, and z directions, and matrix $\tilde{\mathbf{L}}$ collects the vibrational eigenvectors $\tilde{\mathbf{l}}_\mu$ as its columns ($\mu = 1, ..., N_{vib}$). Λ is a diagonal matrix with the eigenvalues λ_μ, leading to the static (harmonic) vibrational frequencies ω_μ according to $\lambda_\mu = 4\pi^2 c^2 \omega_\mu^2$. The tilde symbol stands for mass weighting. The normal mode eigenvectors and eigenvalues are obtained by diagonalizing the force constant matrix $\mathbf{F}^x$ defined in eq 1 according to $\tilde{\mathbf{L}}^\dagger \mathbf{F}^x \tilde{\mathbf{L}} = \Lambda$ with the normalization condition $\tilde{\mathbf{L}}^\dagger \mathbf{M} \tilde{\mathbf{L}} = \mathbf{I}$. The normal mode vectors $\tilde{\mathbf{l}}_\mu$ can be renormalized[43] so that eq 1 is rewritten as

$$\mathbf{F}^x \mathbf{L} = \mathbf{M} \mathbf{L} \Lambda \tag{2}$$

The solution of eq 2 leads to the diagonal normal force constant matrix $\mathbf{K}$ and the reduced mass matrix $\mathbf{M}^R$ in normal

coordinates Q, respectively, with the dimension of matrices K and M^R being $N_{vib} \times N_{vib}$.

$$L^{\dagger} F^x L = K \tag{3}$$

$$L^{\dagger} M L = M^R \tag{4}$$

One can also work in the space of internal coordinates q instead of Cartesian coordinates x. In this case, the Wilson equation[43] becomes

$$F^q D = G^{-1} D \Lambda \tag{5}$$

where D collects the normal mode vectors d_μ ($\mu = 1, ..., N_{vib}$) column-wise and the Wilson matrix G, which is defined as

$$G = B M^{-1} B^{\dagger} \tag{6}$$

whose inverse represents the kinetic energy in terms of internal coordinates. The elements of the rectangular B matrix in eq 6 are given by the partial derivatives of internal coordinates q_n ($n = 1, 2, 3, ..., N_{vib}$) with regard to Cartesian coordinates x_i ($i = 1, 2, 3, ..., 3N$),

$$B_n = \frac{\delta q_n(x)}{\delta x_i} \tag{7}$$

The B matrix is of key importance for the Wilson equation of spectroscopy because it connects different sets of coordinates (internal, symmetry, curvilinear, etc.)[48−50] or Cremer-Pople ring puckering coordinates,[51] with the Cartesian coordinates.[43] Hence, whenever a new set of coordinates is introduced, the first step is to obtain the appropriate B matrix. Because $D^{\dagger} G^{-1} D = M^R$, eq 5 leads to the equivalent of eq 3

$$D^{\dagger} F^q D = K \tag{8}$$

The transformation to normal coordinates Q leading to the diagonal force constant matrix K collecting normal vibrational force constants and matrix D collecting the normal mode vectors d_μ in internal coordinates is a standard procedure in modern quantum chemistry packages.[52] In particular, normal mode stretching force constants have become a popular measure of bond strength. However, a caveat is appropriate. Based on the mathematical framework constructed by Wilson,[23] normal coordinates Q turn out to be a linear combination of internal coordinates q or Cartesian coordinates x

$$Q_\mu = \sum_j^{N_{vib}} (\tilde{D}^{\dagger} G^{-1})_{\mu j} q_j \tag{9}$$

$$Q_\mu = \sum_j^{3N} (\tilde{D}^{\dagger} G^{-1} B)_{\mu j} x_j \tag{10}$$

culminating in the general delocalization of normal vibrational modes over the molecule, which limits the direct use of normal-mode frequencies and normal mode force constants as bond strength measure. Hence, local vibrational modes a_n and related local mode frequencies ω_n^a and force constants k_n^a are needed. Konkoli and Cremer[24,26−31] derived local vibrational modes a_n from the diagonal force constant matrix K and the normal mode vectors d_μ

$$a_n = \frac{K^{-1} d_n^{\dagger}}{d_n K^{-1} d_n^{\dagger}} \tag{11}$$

where the local mode a_n is expressed in terms of normal coordinates Q and d_n is the n-th row vector of the D matrix. For a comprehensive derivation and discussion the reader is refereed to a recent review article.[24]

To each local mode a_n a corresponding local mode force constant k_n^a

$$k_n^a = (d_n K^{-1} d_n^{\dagger})^{-1}, \quad d_n = B_n L \tag{12}$$

and local mode frequency ω_n^a can be defined as follows:

$$\omega_n^a = \frac{1}{2\pi c} \sqrt{\frac{k_n^a}{m_n^a}} \tag{13}$$

The local mode mass, m_n^a, of mode n is given by

$$m_n^a = 1/G_{n,n} = (B_n M^{-1} B_n^{\dagger})^{-1} \tag{14}$$

where $G_{n,n}$ is the n-th diagonal element of the Wilson G matrix. For a chemical bond A−B, eq 14 leads to $M_A M_B/(M_A + M_B)$, whose form is the same as that of the reduced mass of diatomic molecules.

There exists an important one-to-one relationship for each complete set of local vibrational modes and normal vibrational modes, the ACS,[33] which is based on the Decius compliance matrix,[53] $\Gamma = (F^q)^{-1}$, defined as the inverse of the Hessian matrix in internal coordinates, and the Wilson G matrix, $G = B M^{-1} B^{\dagger}$, which is called an inverse kinetic energy matrix:[43]

$$(G_d + \lambda G_{od}) R_\lambda = (\Gamma_d + \lambda \Gamma_{od}) R_\lambda \Lambda_\lambda \tag{15}$$

where G_d and Γ_d and G_{od} and Γ_{od} are the diagonal and off-diagonal parts of Decius and Wilson matrices, respectively.[43] The matrix Λ collects the harmonic vibrational frequencies and $R = \Gamma^{-1} D$. The parameter λ adiabatically converts the local vibrational modes ($\lambda = 0$) into their normal mode counterpart ($\lambda = 1$). As shown in eq 10 normal coordinates are linear combinations of internal coordinates. Therefore, the important role of λ is to smoothly transition from the one-dimensional space of the local modes to the multivariate space spanned by the normal modes.

This one-to-one relationship forms the basis for a new way of interpreting vibrational spectra, the so-called CNM procedure in which each normal vibrational mode l_μ is decomposed into local mode contributions.[24,28−30] For this aim, the local modes a_n in internal coordinates are transformed into their Cartesian coordinate counterparts a_n^x via

$$a_n^x = L a_n = L \frac{K^{-1} d_n^{\dagger}}{d_n K^{-1} d_n^{\dagger}} \tag{16}$$

Then the overlap $S_{n\mu}$ is the overlap between each local mode vector a_n^x and a normal mode vector l_μ is calculated according to

$$S_{n\mu} = \frac{(a_n^x, l_\mu)^2}{(a_n^x, a_n^x)(l_\mu, l_\mu)} \tag{17}$$

with the metric (a, l) given by

$$(a, l) = \sum_{i,j} a_i F_{i,j}^x l_j \tag{18}$$

where $F_{i,j}^x$ is an element of the Hessian matrix F^x in Cartesian coordinates. The contribution $C_{n\mu}$ (local mode character) of

the local vibrational mode $\mathbf{a}_n$ to normal vibrational mode $\mathbf{l}_\mu$ can then be calculated via

$$C_{n\mu} = \frac{S_{n\mu}}{\sum_m^{N_{vib}} S_{m\mu}} \qquad (19)$$

New Protocol. The complete, nonredundant set of N_{vib} local vibrational mode parameters for each of the 11 test examples shown in Figure 1 was generated with our new module LModeAGen, which is based on the molecular connectivity matrix, as described in the pseudocode in Algorithm 1, see Chart 1.

Chart 1. Algorithm 1: Pseudocode for module LModeAGen

```
Algorithm 1 Pseudocode for module LModeAGen
procedure LOCAL MODE PARAMETER GENERATOR
    Geometry information ← read from input file
    Connectivity information ← read from input file
    if Connectivity information = missing then
        Load atomic database
        Build connectivity matrix
    end if

    Convenient Graph analysis ← Internal proper ordering of atoms

    Local Mode parameters ← Graph analysis
    while i,j ≤ Nconnectivity do                    ▷ connectivity indexes
        Gen B(i,j) for connected atoms
        Save the list (Clist) with atom index of B(i,j) closing cycles
    end while
    while i,j,k ≤ Nconnectivity do                  ▷ connectivity indexes
        i ≥ 3 → Gen A(i,j,k) for connected atoms
        Avoid atoms in Clist
    end while
    while i,j,k.l ≤ Nconnectivity do                ▷ connectivity indexes
        i ≥ 4 → Gen D(i,j,k,l)
        if v_ij ∠ v_jk − 180.0 ≤ thold then
            Search for other k value                ▷ Avoids singular dihedrals
            if Other k not found then
                Define degenerate A(i,j,k) and A'(i,j,k)
            end if
        end if
    end while
end procedure
```

The underlying basics and protocol of LModeAGen can be summarized as follows:

- In the LModeAGen protocol, each LVM parameter is considered as a path with up to four vertices (connected by three edges) determined from the molecular connectivity matrix.
- The algorithm generates a set of $(N_B = N − 1)$, $(N_A = N − 2)$, and $(N_D = N − 3)$ local mode parameters $[N_B, N_A, N_D]$ amounting to N_{vib}, with N_B, N_A, and N_D corresponding to the number of bonds, bond angles, and dihedral angles, respectively, following previous guidelines developed in our group,[24,31,33] leading to chemically meaningful LVM results. This holds for any nonlinear polyatomic system and/or molecule without linear subsystems; any noncyclic system and/or without cyclic fragments.
- For molecules with N_{lsub} linear subsystems, degenerate angles are represented by one bond and two angle paths instead of one path for bond, angle, and dihedral. As a consequence, a set with $N_B = N − 1$, $N_A = N − 2 + N_{lsub}$, and $N_D = N − 3 − N_{lsub}$ paths is obtained.
- For systems with N_{cycles} cycles, $N_B = N − 1 + N_{cycles}$ local mode bond parameters are generated. Here, cycles stand for molecular graph defining closed path fragments. $N_A = N − 1 − N_{cycles}$ local mode bond angles parameters are generated, and $N_D = N − 3$ local mode dihedral angles

parameters are generated. Same rules of linear subsystems may apply.

- The direction of the edges is of paramount importance, given that LVMs parameters are used to generate angles and dihedral angles between vector quantities. Each path $(a−d)$, where each entry corresponds to an atomic index in the molecular connectivity matrix (defining the graph), satisfies the relation $a \neq b \neq c \neq d$.

Computational Details. All geometry optimizations and subsequent normal vibrational frequency calculations for molecules **1−10** and NgbCO in the H64ε tautomeric form of distal histidine **11** (see Figure 1) were performed with *Gaussian 16*,[52] utilizing an ultrafine integration grid[54] and a tight convergence criterion for the SCF procedure. The ωB97X-D/aug-cc-pVDZ[55−57] and M06L/def2-TZVP[58,59] levels of theory were adopted for molecules **1−8**, and **9−10**, respectively. NgbCO **11** was computed at the QM/MM ωB97X-D/6-31G(d,p)/AMBER level of theory[55,60,61] utilizing the ONIOM[62] methodology starting from the experimental X-ray structure of carboxy murine neuroglobin[63] (PDB entry: 1W92). It has to be noted that the QM/MM description considers electrostatic and steric interactions between the active site of the heme protein and the entire protein environment. Further details on the QM/MM calculations can be found in the Supporting Information. Starting geometries for **2**, **5**, and **7−10** and the corresponding model chemistries were adapted from ref 35. ACS and CNM were performed with the standalone LModeA package.[64] For the test example **11**, the normal vibrational modes of the QM subsystem were extracted from the full QM/MM set of normal modes vibrations using the GSVA procedure developed in our group.[41,42]

RESULTS AND DISCUSSION

Table 1 summarizes the results obtained for test examples **1−11**, covering molecules with different symmetry and an increasing number of atoms. All local mode parameters were obtained with our new automatic protocol and all LVMs discussed in the following are based on these local mode parameters. ACS plots herein discussed (see Figures 2−12, 15, 16, and 17−19) are presented in a form that the left-hand side collects the LVMs ($\lambda = 0$, one-dimensional space of LVM) and the right-hand side collects the NVMs ($\lambda = 1$, multivariate space of NMV), with different LVMs grouped by chemical similarity and colored accordingly in each figure. In the Supporting Information, CNM plots can be found in Figures S1−S10, as well as the QM/MM methodology, the Cartesian coordinates, and a description of the NVM movies of test examples **1−11**.

Linear Systems. Test example **1**, the linear CO_2 molecule in the fundamental $D_{\infty h}$ state, has four NVMs. The two-degenerate Π_u NVMs describe the O=C=O bending vibrations. They exhibit 100% local O—C—O vibrational mode character, as shown in Table 1 and Figure S1, Supporting Information. The ACS shown in Figure 2 provides the same picture, the two degenerate local O—C—O modes (red line in Figure 2) transform 100% into their NVM counterparts. On the other hand, the two equivalent C=O stretching LVMs (Figure 2, blue line) split up into the Σ_g and Σ_u C=O bond stretching NVMs, with a 50% contribution to each of these two NVMs (see Figure S1, Supporting Information). This example clearly shows that the new

Table 1. Results for Test Examples 1−11[a] (See Figure 1); Point group; Nonredundant Set of LVM Parameters: N_B Bonds, N_A Bond Angles, and N_D Dihedral Angles Adding up to N_{vib}, Determined by LModeAGen; for Selected NVMs, Symmetry, Normal Mode Frequency $\tilde{\nu}$ (in cm^{-1}); Dominant LVM Parameters and Their Contributions (in %), Determined by CNM[b]

| molecule | point group | LVM parameter set | | selected normal vibrational modes | | | |
		N_{vib}	$[N_B, N_A, N_D]$	sym.	$\tilde{\nu}$	LVMs	%
1	$D_{\infty h}$	4	[2, 2, 0]	Π_u	682	O−C−O	100
2	C_{2v}	6	[3, 2, 1]	B_1	1208	H−C−O−H	100
				A_1	1842	O−C	92
3	C_S	6	[3, 2, 1]	A''	1037	H−C−O−F	100
				A'	1356	O−C−H	98
				A'	1908	O−C	93
				A'	3122	C−H	98
4	D_{6h}	30	[12, 9, 9]	E_{2u}	414	C−C−C−C	37
				E_{2g}	622	C−C−C	51
5	C_S	33	[13, 10, 10]	A'	3906	H−O	100
				A'	3186	H−C	86
				A''	365	H−O−C−C	97
6	C_S	33	[13, 10, 10]	A'	3903	H−O	100
				A''	332i	H−O−C−C	93
7	C_3	99	[37, 30, 32]	A	2225	H−Si	100
8	C_3	108	[40, 33, 35]	A	1295	O−P	82
9	C_{4v}	111	[46, 30, 35]	A_1	2058	O−C	93
				A_1	576	C−Fe	88
				E	535	O−C−Fe	49
				E	535	O−C−Fe	44
10	C_1	138	[56, 38, 44]	A	3663	N−H	100
				A	2063	O−C	95
				A	826	H−C−N−Fe	81
				A	497	C−Fe	78
11	C_1	285	[106, 85, 94]	A	3697	N−H(proximal)	100
				A	3670	N−H(distal)	99
				A	2148	O−C	94
				A	861	C−N−Fe	81
				A	830	H−C−N−Fe	91

[a]ωB97X-D/aug-cc-pVDZ and M06L/def2-TZVP levels of theory for test examples **1−8**, and **9−10**, respectively. Test example **11** was calculated at the QM/MM ωB97X-D/6-31G(d,p)/AMBER level of theory. [b]Figures S1−S10, Supporting Information, provide more details on CNM analyses and movies that show the corresponding movements of the atoms during the NVMs.
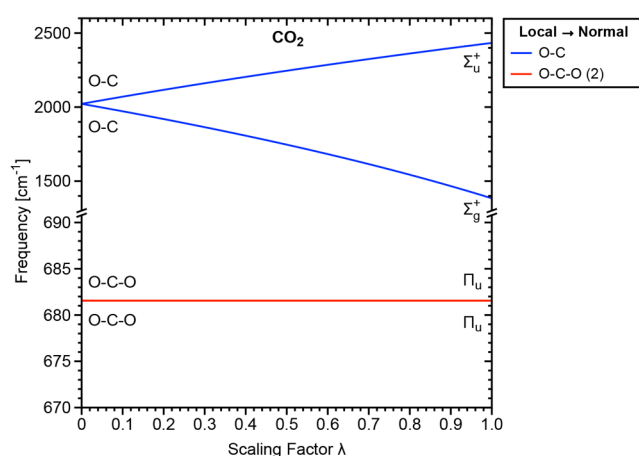

Figure 2. ACS plot of test example **1** relating local mode frequencies (left) with normal-mode frequencies (right). ωB97X-D/aug-cc-pVDZ level of theory.

algorithm automatically identifies linear molecules or subsystems in order to generate degenerate local mode parameters and the correct number of N_{vib} local mode parameters.

Formaldehyde and Formyl Fluoride. The normal vibrational out-of-plane bending mode of test example **2** (formaldehyde H$_2$CO, C_{2v} symmetry), corresponding to the lowest normal vibrational mode frequency ($\tilde{\nu} = 1208$ cm^{-1}, B_1 symmetry, see Table 1) has 100% local H−C−O−H dihedral angle character (see Figure S2, Supporting Information). The B_2 symmetric rocking NVM ($\tilde{\nu} = 1256$ cm^{-1}) and the A_1 symmetric CH$_2$ bending NVM ($\tilde{\nu} = 1522$ cm^{-1}) are adiabatically connected to two equivalent H−C−O angle LVMs, as shown in the ACS plot in Figure 3a, with a 50%−50% and 46%−46% composition, respectively (Table 1 and Figure S2, Supporting Information). In previous work,[35] both H−C−O angles were combined to one local mode parameter leading to CNM percentage values of 100% and 95% for bending and rocking NVMs, which basically sum up to the contributions obtained for the H−C−O−H dihedral angle used in this work. The A$_1$ symmetric C=O NVM is adiabatically connected to the O = C LVM, with a composition of 92% in line with previous work on the assessment of the C=O stretching vibration as a suitable Stark effect probe.[35] The two nondegenerate symmetric and asymmetric C−H stretching NVMs are connected to two equivalent H−C LVMs, with a 50%−50% composition.
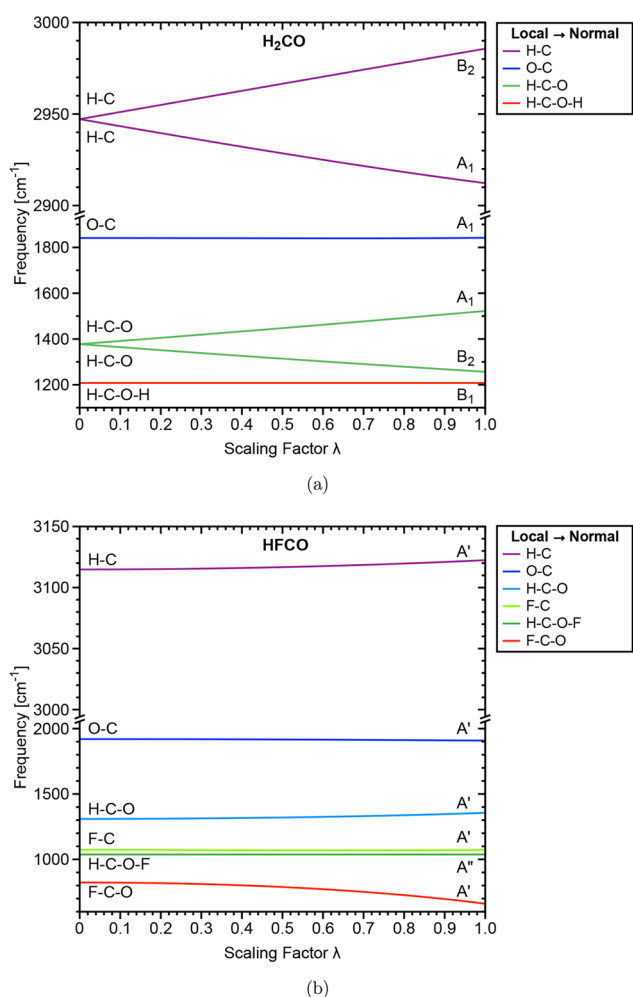
Figure 3. ACS plots of test examples (a) **2** (H$_2$CO) and (b) **3** (HFCO) relating local mode frequencies (left) with normal-mode frequencies (right). ωB97X-D/aug-cc-pVDZ level of theory.

Formyl fluoride, test example **3**, C_S symmetry, has the same amount of NVMs (six) as formaldehyde. Similar to the isotopic effect reported by McKean,[65] the F-substituent related vibrational modes exhibit lower vibrational frequencies compared to their lighter counterparts. As a consequence, three main effects are observed: (i) Breaking of degeneracy; (ii) Increase in normal mode localization; (iii) Decrease in normal-local coupling frequencies,[31,33] as can be seen in Figure 4. The normal out-of-plane bending mode in **3** appears with frequency 1037 cm^{-1} being ca. 220 cm^{-1} smaller than the same mode in **3** due to the presence of the heavier F atom. Nevertheless, CNM percentages reveal that this NVM has 100% local H–C–O–F dihedral angle character (Figure S3, Supporting Information). The formyl fluoride C=O stretching normal mode with a normal-mode frequency at 1908 cm^{-1} is composed of 93% O=C LVM bond stretching, that is, again a good Stark effect probe. The local H–C stretching and the local H–C–O bending parameters with 50%/50% CNM contributions in **2** are drastically affected by the symmetry breaking due to the substitution of one hydrogen atom with fluorine. The C–H NVM connected to a frequency of 3122 cm^{-1} has now 98% local CH character and the corresponding C–F NVM connected to a frequency of 1072 cm^{-1} has 74% local C–F character. The normal mode H–C–O bending (at 1356 cm^{-1}) has 98% local H–C–O character and the corresponding normal F–C–O bending (at 1072 cm^{-1}) has 74% local F–C–O character, (see CNM bar diagrams in Figure S3). The high localization of formyl fluoride (test example **3**) NVMs can also be seen in the ACS plot in Figure 3b which shows very small variation of normal-mode frequencies and their local frequencies counterparts (i.e., small coupling frequencies[31,33]).

LModeAGen generates the same graphs for tests examples **2** and **3**, leading to the exact same set of LVM parameters. The differences observed in CNM and ACS are due to the chemical difference between the two systems. As a result of F substitution, an electron-withdrawing effect is observed,
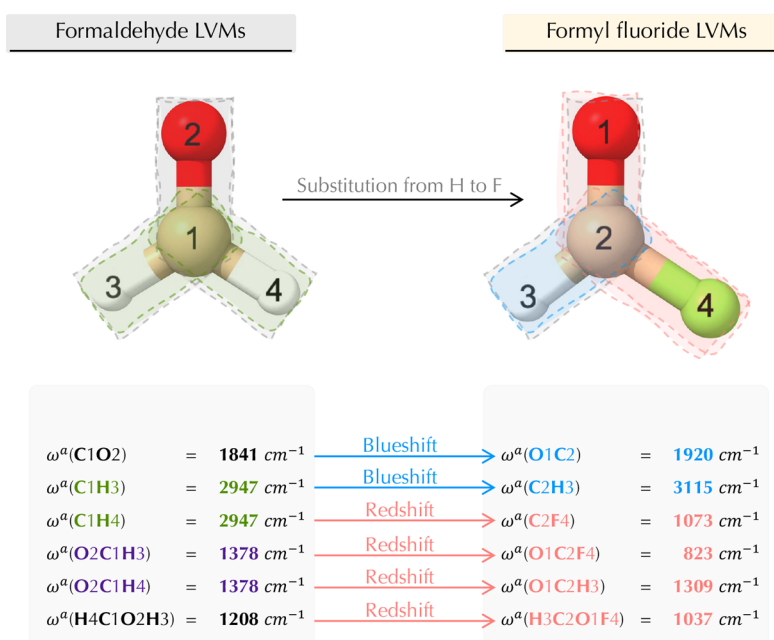

Figure 4. LVMs of test examples **2** (H$_2$CO) and **3** (HFCO) indicating changes upon H to F substitution. ωB97X-D/aug-cc-pVDZ level of theory.
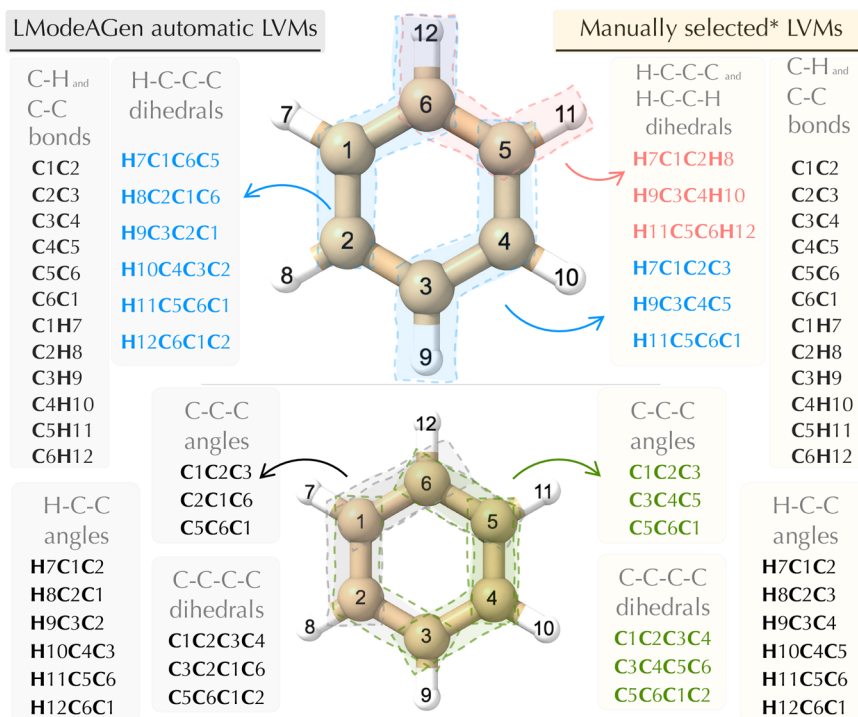
Figure 5. LVM parameters that were automatically generated by LModeAGen (left) and extracted from the literature[33] (right) for benzene in the D_{6h} point group. Herein, H−C−C−C and C−C−C LVMs obtained by LModeAGen are contrasted with H−C−C−C, H−C−C−H, and C−C−C LVMs from the literature.

which is followed by a blue shift (increase in local mode frequency) for the C−H bond in the O=C−H fragment when comparing formaldehyde and formyl fluoride molecules (see Figure 4). C−H LVMs in formaldehyde appear with local frequency at 2947 cm⁻¹, changing to 3115 cm⁻¹ in formyl fluoride molecule. On the other hand, H−C−C LVMs in formaldehyde appear with local frequency at 1378 cm⁻¹, red shifting to 1309 cm⁻¹ in formyl fluoride molecule. A similar trend was observed for benzene and its fluorine-substituted counterpart,[66] in which H to F substitution causes a blue shift in *ortho-*, *meta-*, and *para-*locations C−H bonds and a red shift in LVM C−C−C angular distortion. Also, the formyl fluoride O=C bond is stronger (k^a = 14.89 mDyn/Å) than the formaldehyde O=C bond (k^a = 13.69 mDyn/Å) counterpart.

Benzene: LModeAGen and Reference LVM Parameters. Besides being a challenging case for the determination of LVM parameters, the highly symmetric benzene molecule **4** is also an important test case since it may serve as a building block for larger annulated ring systems. The relationship between normal and a complete set of nonredundant local vibrational modes for benzene was reported previously,[27,33] establishing a reference for benzene LVMs. Figure 5 depicts two sets of LVM parameters, one obtained with LModeAGen and the other extracted from previous work[33] (from this point on referred to as LModeAGen and reference, respectively). Figure 6a−k depicts displacement vectors for selected benzene NVMs, while Figures 7a,b, 8a,b, and 9a,b illustrate CNM plots for LModeAGen and reference LVM parameters.

The comparison between LModeAGen and reference parameters lead to the identification of differences in some normal mode compositions as combinations of local modes (changes in CNM characteristics of some normal modes). The main difference between LModeAGen and reference parameters for benzene is how the hydrogen out-of-plane distortions

are described. While three H−C−C−H and three H−C−C−C dihedral LVMs are defined in the reference set,[33] LModeAGen automatically generated six equivalent torsion H−C−C−C. Konkoli, Larsson, and Cremer[27] reported benzene LVM parameters similar to LModeAGen, with six C−C, six C−H, six H−C−C, three C−C−C, three C−C−C−C, and six H−C−C−C, where the H−C−C−C reported by Konkoli are of bond-plane type dihedrals and LModeAGen generated torsion dihedrals.

The choice of substituting three H−C−C−C with H−C−C−H dihedrals lead to a different description of the most intense infrared (IR) active benzene NVM (A_{2u} in Figure 6e) assigned to H−C−C−C symmetric out-of-plane distortion. All hydrogen out-of-plane movements participate equally in this mode. The six-degenerate H−C−C−C generated by LModeAGen equally compose the NVM with frequency at 690 cm⁻¹ (Figures 7a,b and 6e), while the reference set produces a CNM composed only by three H−C−C−H dihedral LVMs. In the reference set, H−C−C−H was defined in such way that all six H atoms are defined in these three dihedrals (see right-side H−C−C−H in Figure 5), leading to an apparent larger localization of CNM.

The choice of C−C−C angles also influence the CNM percentages. LModeAGen, reference,[33] and Konkoli[27] C−C−C parameters sets are equivalent in the description of NVMs attributed to the in-plane C−C−C ring deformations (see Figure 6c,d). These modes should be described by symmetry equivalent C−C−C LVMs, which is not observed in the CNM plots in Figure 7, where, as an example, C2C1C6 (for LModeAGen) and C3C4C5 (for reference) is composed of 51% LVM at the second NVM with frequency at 622 cm⁻¹. Although LModeAGen and reference utilize different choices of C−C−C angles, both sets lead to equivalent CNM percentages (not covering symmetry aspects) of these
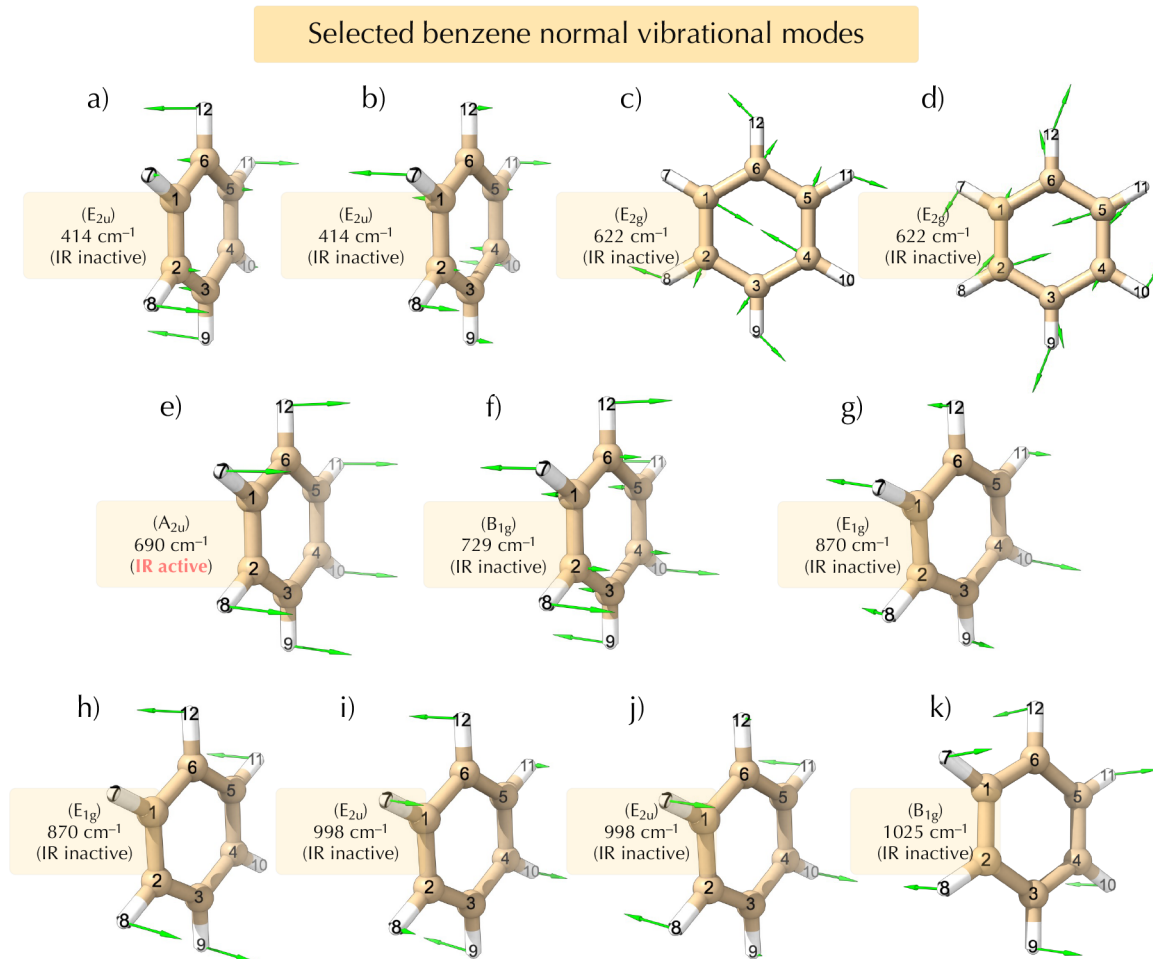
Figure 6. Displacement vectors for selected NVMs involving (a, b) C−C−C−C out-of-plane distortions; (c, d) C−C−C in-plane, and (e−h) C−C−C−C out-of-plane distortions for benzene in the D_{6h} point group obtained at the ωB97X-D/aug-cc-pVDZ level of theory. Symmetry, normal-mode frequency $\tilde{\nu}$ (in cm^{-1}) and IR activity are indicated.

modes. To represent these two in-plane C−C−C movements in these two degenerate NVMs, a set of four C−C−C angles should be defined involving the atoms participating in the displacements seen in Figure 6c-d, which would have a consequence with withdrawing some of the other LVMs. Generally, all NVMs in which H out-of-plane motions are involved show different compositions when comparing the sets of LModeAGen and reference parameters (see Figures 7a,b and 6f−k). Among these modes, the E_{1g} NVM (Figure 6h) is attributed to four H−C−C−C equal movements. The CNM plot obtained from the LModeAGen set (see second NVM with frequency at 870 cm^{-1} in Figure 7a) describes this symmetry equivalence better than the set from the reference (Figure 7b). The B_{1g} NVM (Figure 6k), with a frequency at 1025 cm^{-1}, also reflects the symmetry break in CNM due to the difference of having three H−C−C−H, three H−C−C−C, and six H−C−C−C dihedrals, as can be seen when comparing CNMs in Figure 8a,b.

There is one C−C−C−C dihedral LVM parameter that differs between the LModeAGen and reference sets. Within both sets, the B_{2u} NVM at 1012 cm^{-1} (see Figure 8a,b) is mainly composed of three C−C−C−C dihedral LVMs, which are equivalent for LModeAGen and reference sets, making it clear that, although there were two different sets of parameters, each equally describe the molecular motion related to C−C−

C−C dihedral distortions. The two-degenerate E_{2u} NVMs, with frequencies at 414 cm^{-1}, are mainly composed of C−C−C−C dihedral LVMs (see Figure 7a,b) for both LModeAGen and reference sets. However, these two NVMs also have contributions from different H−C−C−C dihedral distortions, as shown in Figure 6a,b. This aspect explains the difference between LModeAGen and reference sets in the CNM plots.

The parameters for H−C−C angle LVMs differ in the third atom (see left and right H−C−C angles in Figure 5). All of these LVMs (from LModeAGen and reference) are degenerate and equivalent by symmetry. The parameters for C−C−C angle LVMs are also slightly different when the LModeAGen ouput is compared with the reference counterpart, differing by one C−C−C angle. As depicted in Figure 5, the reference C−C−C angle LVMs are manually selected to be more spread out in the ring (only sharing one atom per angle), and this imposition was not explicitly implemented in LModeAGen algorithm. All parameters for C−C and C−H bond LVMs are equal in both sets (see Figure 5). The similarity and symmetry equivalence of C−C, C−H, H−C−C, and C−C−C LVMs lead to identical CNM plots in NVMs composed by these LVMs (nomal modes with frequencies at 622 cm^{-1} in Figure 7a,b, range 1030−1462 cm^{-1} in Figure 8a,b, and all normal modes in Figure 9a,b). The optimization of LVMs parameters regarding symmetry, thermodynamic and other aspects is
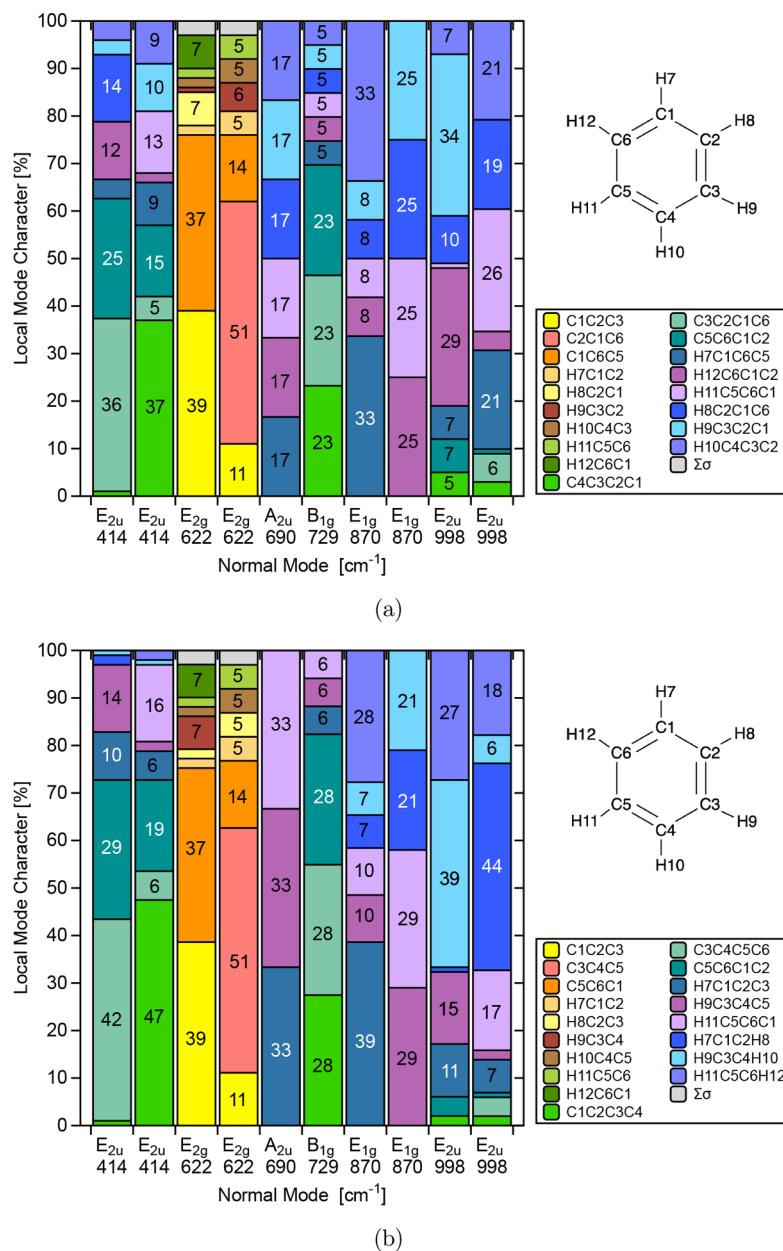
(a)

(b)

Figure 7. (a) LModeAGen and (b) ref 33 CNM plots (NVMs 1−10) of benzene at the ωB97X-D/aug-cc-pVDZ level of theory. $\Sigma\sigma$ comprises the summation of all of the σ local mode contributions below the threshold of 1%.

currently in progress. In this regard the LModeAGen parameter set can be considered as a solid starting point.

Benzene and Phenol. Figures 10, 11, and 12 show ACS plots for benzene **4**, planar phenol **5** (C_S symmetry, minimum), and phenol **6** (C_S symmetry, transition state (TS) for OH rotation; see Figure 1). LModeAGen, while analyzing benzene and phenol graphs, identifies that a closed path is present (in these cases, the six-member ring) and, for the atom with the higher index in the closed path, an additional bond LVM is defined (and as a consequence no angle is defined starting from this atom, satisfying the condition 4 in "New Protocol" section). In benzene and phenol molecules presented here, the internal order definition of LModeAGen makes C4 being the one to close the paths. It must be emphasized that C4 participates of LVMs parameters (see Figure 5), but not being present as the first or last in the order of C−C−C angles. This

means that C4 is not used by LModeAGen to generate any angle LVM parameter, but C4 appear in the definitions made using other atoms.

LModeAGen identified for benzene six C−C, six C−H, six H−C−C, three C−C−C, three C−C−C−C, and six H−C−C−C. Benzene **4** has 30 NVMs which are adiabatically connected to 6 groups of degenerate LVMs, as shown in Figure 10. The algorithm automatically generated three C−C−C−C bond dihedral angles (at local frequency 602 cm^{-1}), six H−C−C−C bond dihedral angles (at local frequency 791 cm^{-1}), three C−C−C bond angles (at local frequency 1287 cm^{-1}), six C−C bond stretching (at local frequency 1378 cm^{-1}), and six C−H bond stretching (at local frequency 3206 cm^{-1}). Given the high symmetry, the normal modes are generally delocalized and described by all LVMs of some fragment group. E_{2u} C−
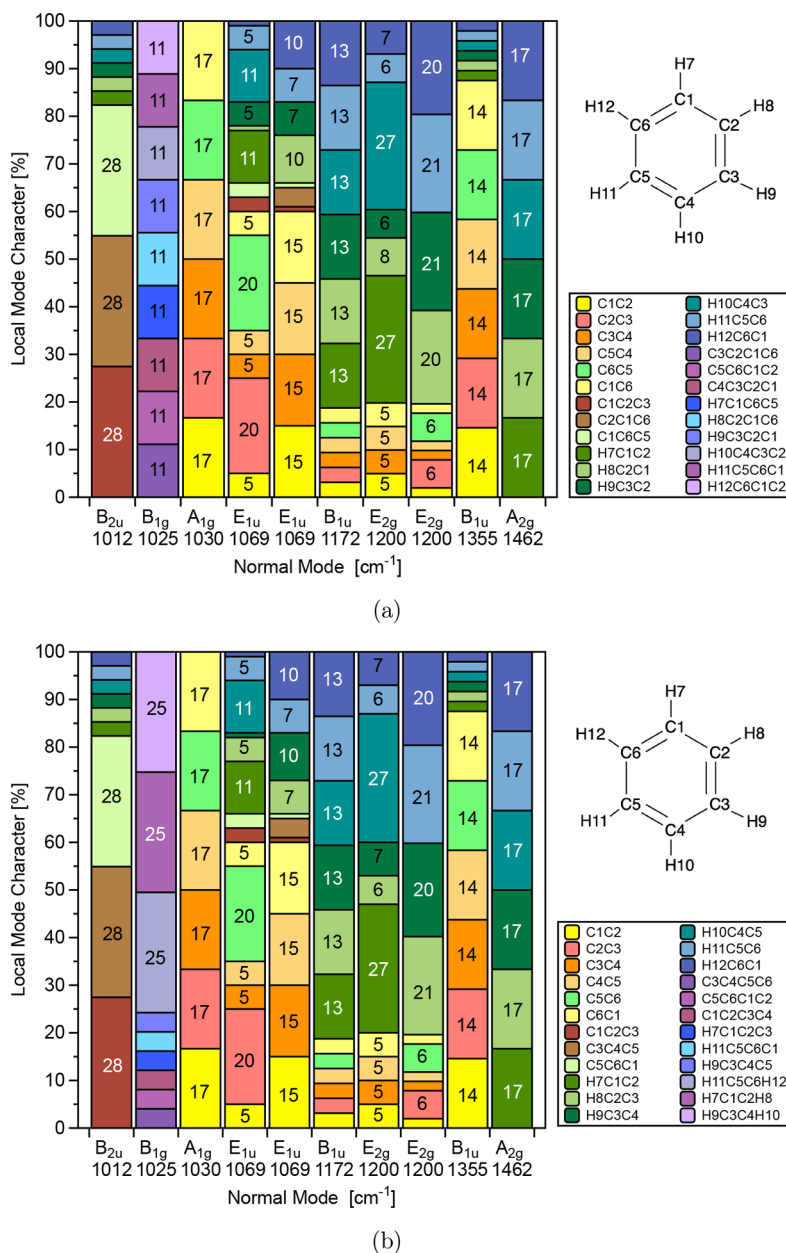
Figure 8. (a) LModeAGen and (b) ref 33 CNM plots (NVMs 11−20) of benzene at the ωB97X-D/aug-cc-pVDZ level of theory.

C−C−C out-of-plane and E_{2g} C−C−C in-plane deformations are the most localized NVMs (see Table 1 and Figure 7a).

The comparison between benzene and phenol molecules reveals the consistency of our LVM parameters generator and the sensibility of these parameters in the case of symmetry breaking. Test example **5**, phenol with C_S planar conformation (Figure 1) has 33 NVMs. In the range 230−1700 cm^{-1}, 27 NVMs are adiabatically connected to six groups of LVMs with local mode frequencies in the range between 346−1390 cm^{-1} (Figure 11), while six NVMs (ca. 3185−3900 cm^{-1}) are connected to a group of six LVMs within a similar frequency range.

The LVMs H−C−C−C, C−C−H, and C−H (with local frequencies at 791, 1287, and 3206 cm^{-1}) that describe one H atom in benzene are substituted by O−C−C−C, C−C−O, and C−O in phenol (with local frequencies at 349, 771, and 1223 cm^{-1}). This result is in line with the expected decrease in

fragment vibrational frequency due to a heavier atom. Also, additional H−O−C−C, C−O−H, and O−H LVMs (with local frequencies at 386, 1281, and 3902 cm^{-1}) are generated to describe H in hydroxyl group. Table 1 shows test example **5** (phenol) CNM results for A', A', and A'' NVMs with frequencies at 3906, 3186, and 365 cm^{-1} being 100%, 86%, and 97% composed by O−H, C−H, and H−O−C−C LVMs, respectively (see Table 1 and Figure S4, Supporting Information). The latter describes hydroxyl group rotation. The rest of LVM parameters generated by LModeAGen are equal to benzene counterpart.

As a result of H to OH substitution, an electron donating effect is observed through the degeneracy break of C−H LVMs frequencies. In benzene, C−H local mode stretching appear as a six degenerate at local frequency 3206 cm^{-1}. Phenol molecule in a minimum conformation exhibit a break of *ortho-* and *meta-* C−H bonds as a consequence of O−H group being directed to
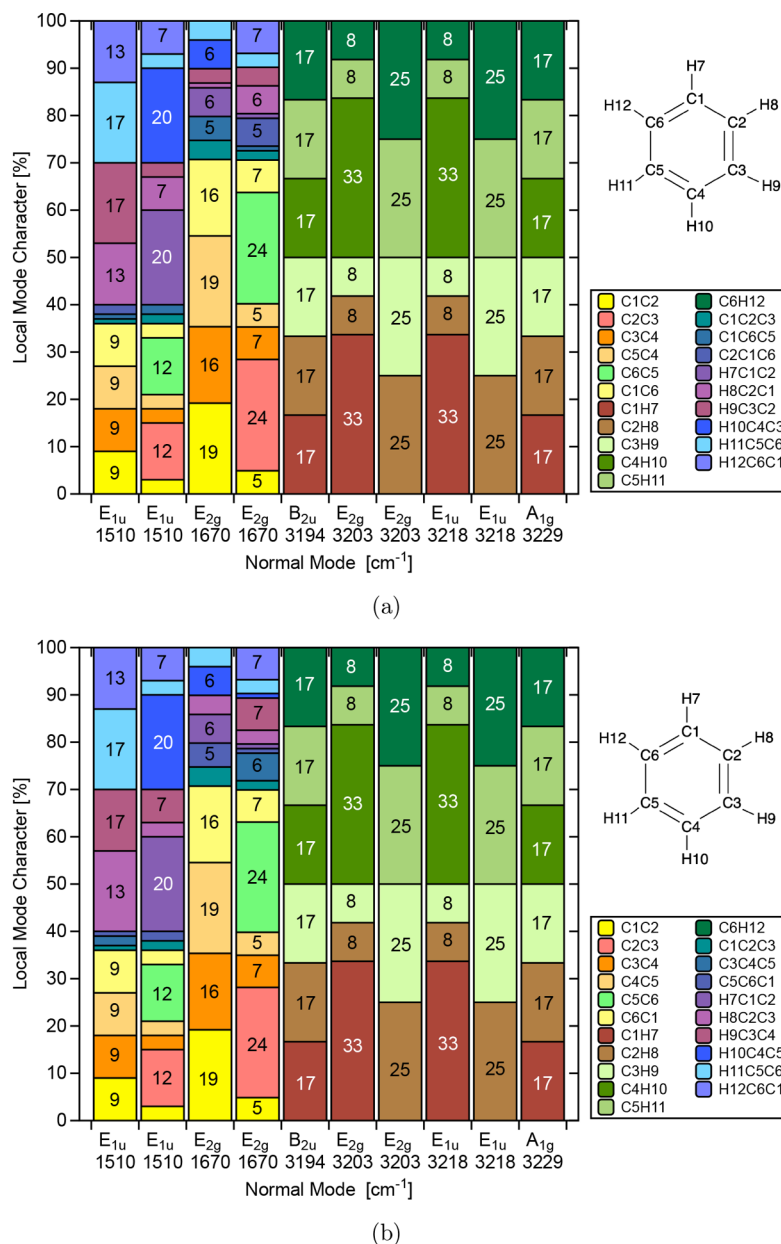
Figure 9. (a) LModeAGen and (b) ref 33 CNM plots (NVMs 21−30) of benzene at the ωB97X-D/aug-cc-pVDZ level of theory.

one of *ortho*-C−H fragment (C1H7 in Figure 13a). In this way, *cis−ortho*-, *trans−ortho*-, *cis−meta*-, and *trans−meta*-locations C−H bonds can be labeled (see Figure 13a) to C−H bonds in different chemical environment. In line with what was previously reported,[66] comparing phenol from benzene, a red shift is observed for LVM *cis−ortho*-C−H bond stretching while blue shifts are observed for *meta*-C−H and *para*-C−H bond stretching, as can be seen in Figure 13a.

Figure 13b depicts phenol in a conformation with the O−H bond perpendicular to the phenyl ring. This is a phenol transition state (phenol-TS, test example **6**) between two equivalent phenol minima similar to test system **5**. In this conformation, unlike the phenol minimum, this phenol-TS exhibits equivalent *ortho*-C−H and *meta*-C−H bonds. LModeAGen generates all LVMs parameters equal to test example **5**. Comparing ACS plot for test example **6** in Figure 12 to test example **5**, it is possible to visualize the main difference: the imaginary normal-mode frequency at 332*i* cm⁻¹

is composed 93% by LVM H−O−C−C bond dihedral deformation. This normal mode is the intrinsic reaction coordinate for the interconversion between phenol minima, having a negative local (and normal) force constant. This local-normal ACS is represented as the negative line in Figure 12. The CNM for phenol TS also reveal NVM with frequency at 3906 cm⁻¹ 100% composed by O−H bond stretching LVM (see Table 1 and Figure S5, Supporting Information).

Triphenylsilane and Triphenyl Phosphate. Test examples **7** and **8**, triphenylsilane and triphenyl phosphate, were calculated in the C_3 point group. As a consequence, phenyl rings in each molecule will have symmetry equivalent molecular fragments (see Figure 14a,b). Ring moieties *cis*- and *trans*- to Si−H bond are in different chemical environments and are found to be nonequivalent. Also, each phenyl group in test examples **7** and **8** can be viewed as interacting with a diphenyl selenide or diphenyl phosphate, respectively. Therefore, *ortho*-, *meta*-, and *para*-positions are also non-
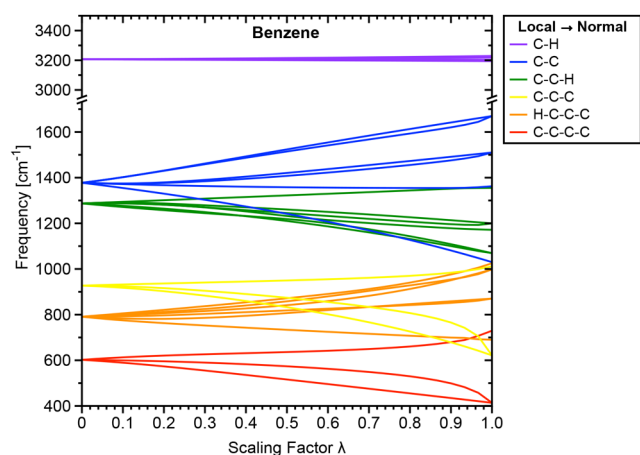
Figure 10. ACS plots of test example **4** (benzene) relating local mode frequencies (left) with normal-mode frequencies (right). Local vibrational modes are indicated, while normal vibrational mode symmetries are suppressed. ωB97X-D/aug-cc-pVDZ level of theory.
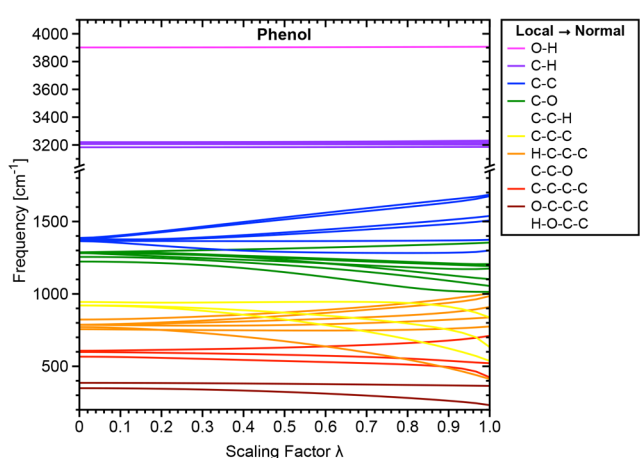

Figure 11. ACS plots of test example **5** (phenol) relating local mode frequencies (left) with normal-mode frequencies (right). Local vibrational modes are indicated, while normal vibrational mode symmetries are suppressed. ωB97X-D/aug-cc-pVDZ level of theory.
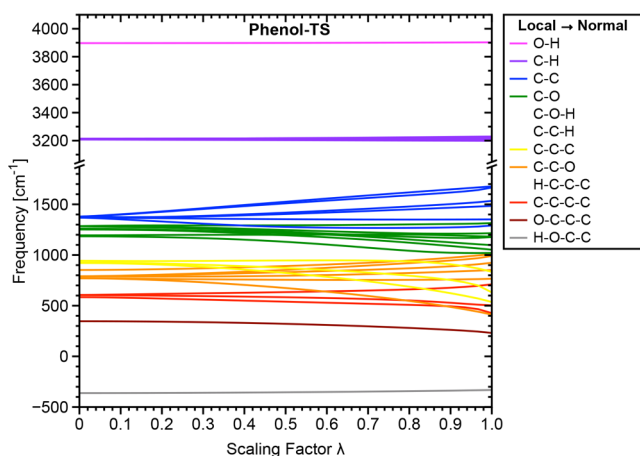

Figure 12. ACS plots of test example **6** (phenol-TS) relating local mode frequencies (left) with normal-mode frequencies (right). Local vibrational modes are indicated, while normal vibrational mode symmetries are suppressed. ωB97X-D/aug-cc-pVDZ level of theory.

equivalent. Due to the C_3 symmetry, LModeAGen automatically generates LVM parameters that are three-degenerate in test examples **7** and **8**. Additionally, Graph paths were generated successfully, recognizing the cycles and leading to the appropriate number of bonds, angles, and dihedral LVM parameters.

As examples, LVM for C−H stretching are depicted in Figure 14a,b as three-degenerate blocks. Compared with benzene (ω^a(C−H) = 3206 cm^{-1}), all LVM C−H stretching in triphenylsilane (Figure 14a) have decreased (red shift) local frequencies in the order: ω^a(*cis−ortho*-C−H) < ω^a(*trans−ortho*-C−H) < ω^a(*trans−meta*-C−H) < ω^a(*cis−meta*-C−H) < ω^a(*para*-C−H) < ω^a(benzene−C−H), with *meta*- and *para*-C−H having almost equivalent ω^a values. This trend is a consequence of the Si−H group as a moderate electron donor[67] to phenyl rings, making C−H bonds (mainly the *meta*-location) weaker. An opposite trend is observed for obtained C−H bond stretching LVMs in triphenyl phosphate (Figure 14b). In this case, the well-known P═O deactivating group (through π-back-donation) directs electrophilic substitution reactions to the meta position.[68,69] Our results are totally in line with this effect, being the local frequency order ω^a(*cis−meta*-C−H) < ω^a(*trans−meta*-C−H) < ω^a(*para*-C−H) < ω^a(*trans−ortho*-C−H) < ω^a(*cis−ortho*-C−H), indicating the *meta*-C−H bonds as the weakest in test example **8**.

The symmetry equivalence of triphenylsilane can also be visualized in groups of degenerate LVMs below 500 cm^{-1} (Figure 15), describing C−C−Si−C different bond dihedrals and C−Si−C bond angle distortions. Nine H−C−C−C dihedral distortions (three for each phenyl group) with local mode frequencies in the range of 783−788 cm^{-1}, and six C−C−C angular distortions with local mode frequencies in the range of 927−929 cm^{-1} are also observed. Fifteen C−C−H angular distortion and 18 C−C bond stretching LVMs have local mode frequencies in ranges of 1285−1320, and 1338−1379 cm^{-1}, respectively.

The H−Si bond stretching vibration with a local mode frequency of 2222 cm^{-1} is adiabatically connected to the normal mode with frequency of 2225 cm^{-1}, with a CNM percentage value of 99.91% (Table 1 and Figure S6, Supporting Information), in line with previous finding that this bond is a qualified vibrational Stark effect probe.[35]

LModeAGen automatically generated for test example **8**, triphenyl phosphate, 12 different groups of quasi-degenerate LVMs adiabatically connected to 108 LVMs, as shown in Figure 16. C−C−O−P and C−O−P−O dihedral distortions appear with local mode local vibrational modes with frequencies that fall within 45−75 cm^{-1}, while six C−C−C−O dihedral distortions appear with local frequencies that fall within 320−329 cm^{-1}. Two other LVM groups, one collecting P−O−C and another collecting O−P−O angles, appear with local mode frequencies in the ranges of 402−406 cm^{-1}, and O−P−O−O dihedrals have local frequencies at 442−473 cm^{-1}. Three C−C−C−C dihedral distortions appear degenerated at 590 cm^{-1}, and six O−C−C angle distortions appear as quasi two-degenerate LVMs with local mode frequencies at 685−696 cm^{-1}.

Each H was analyzed by LModeAGen algorithm to provide one dihedral of H−C−C−C or H−C−C−O types in a group of 15 LVMs with local mode frequencies in the range of 750−790 cm^{-1}. The three C−O bonds give LVMs with a local mode frequency at about 1125 cm^{-1}, while C−C−H angles are collected together with O−P bond LVMs with local mode

C–H stretching
local mode frequencies

$\omega^a(C1H7) = 3183\ cm^{-1}$
$\omega^a - \omega^a(C-H_{benzene}) = -23\ cm^{-1}$

$\omega^a(C4H10) = 3207\ cm^{-1}$
$\omega^a - \omega^a(C-Hbenzen_e) = 1\ cm^{-1}$

$\omega^a(C2H8) = 3207\ cm^{-1}$
$\omega^a - \omega^a(C-Hbenzen_e) = 1\ cm^{-1}$

$\omega^a(C3H9) = 3212\ cm^{-1}$
$\omega^a - \omega^a(C-Hbenzen_e) = 6\ cm^{-1}$

$\omega^a(C5H11) = 3220\ cm^{-1}$
$\omega^a - \omega^a(C-Hbenzen_e) = 14\ cm^{-1}$

(a)

C–H stretching
local mode frequencies

$\omega^a(C2H8) = 3208\ cm^{-1}$
$\omega^a - \omega^a(C-H_{benzene}) = 2\ cm^{-1}$

$\omega^a(C4H10) = 3208\ cm^{-1}$
$\omega^a - \omega^a(C-Hbenzen_e) = 2\ cm^{-1}$

$\omega^a(C3H9) = 3208\ cm^{-1}$
$\omega^a - \omega^a(C-Hbenzen_e) = 2\ cm^{-1}$

$\omega^a(C1H7) = 3214\ cm^{-1}$
$\omega^a - \omega^a(C-Hbenzen_e) = 8\ cm^{-1}$

$\omega^a(C5H11) = 3214\ cm^{-1}$
$\omega^a - \omega^a(C-Hbenzen_e) = 8\ cm^{-1}$
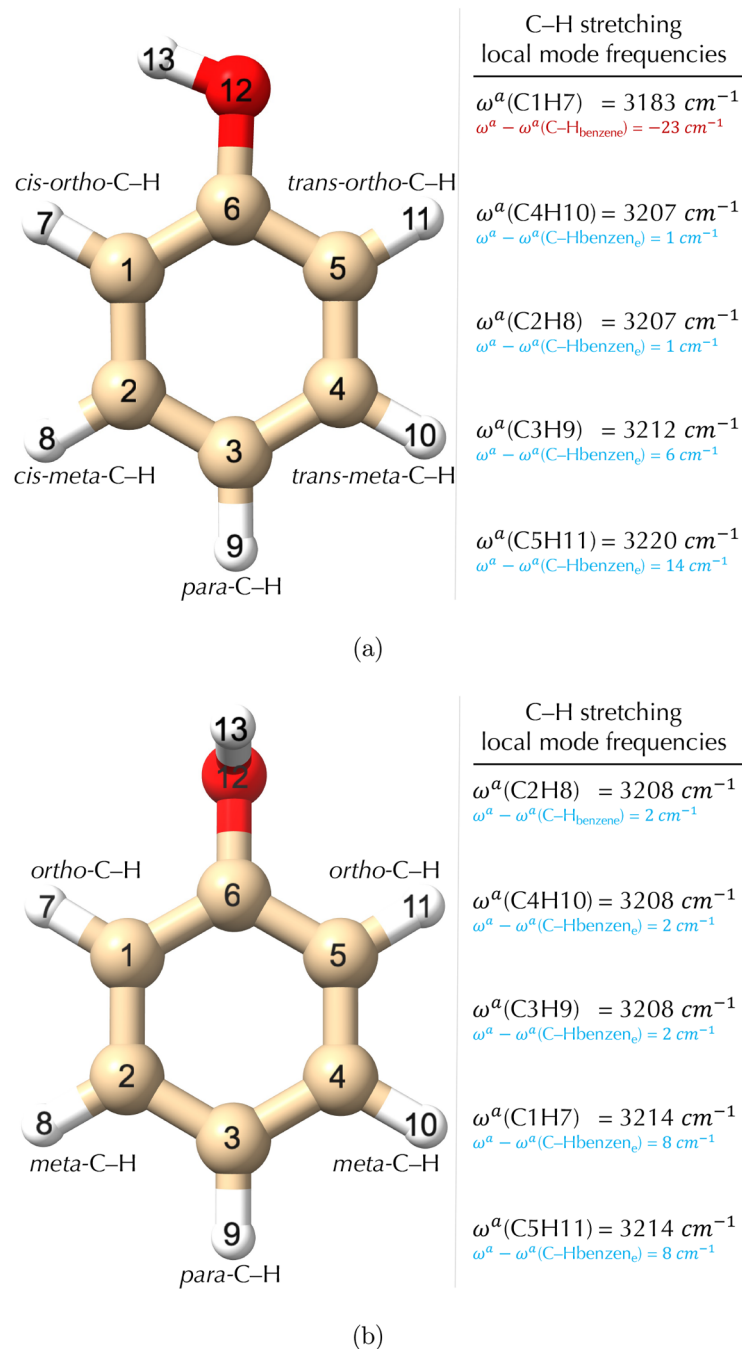
(b)

Figure 13. (a) Phenol minimum and (b) transition state conformations with indications of *ortho-*, *meta-*, and *para*-C−H bonds, their local mode stretching frequencies and differences from C−H bond in benzene counterpart (3206 cm^{-1}).

frequencies in the range of 1250−1290 cm^{-1}. A total of 18 LVM parameters for C−C bonds were automatically generated by LModeAGen and provided six groups of three-degenerate LVMs with local mode frequencies at 1370−1380 cm^{-1}.

Triphenyl phosphate NVMs with higher localization are those with normal-mode frequencies at 1294 cm^{-1} and the most localized NVM is the one with the corresponding normal-mode frequency at 3240 cm^{-1}, whose CNM percentage values correspond mainly to P−O and *ortho*-C−H bond stretching LVMs, respectively (Table 1 and Figure S7 in the Supporting Information).

Ligated Fe(II)-Porphyrins and Carboxy-Neuroglobin. Test example **9** is the ligated Fe(II)-porphyrin FeP−L, with L

= CO, leading to a five-coordinated metal atom. Test example **10** is ligated Fe(II)-porphyrin L′−FeP−L, with L = CO, L′ = imidazole, leading to a six-coordinated metal atom. Test example **11**, the QM subsystem of an active site of carboxy-neuroglobin in the ϵ tautomeric form of distal histidine H64ϵ (NgbCO-QM), presents the largest system investigated in this work. Text examples **9** and **10** were previously reported by our group as qualified vibrational Stark effect probes[35] with highly localized CO NVMs. Whereas the FeC and CO bond strengths in hexacoordinate carboxy-myoglobin[36] and in hexa- and pentacoordinate carboxy-neuroglobin[70] were previously successfully investigated by us, ACS and CNM procedures were not feasible. However, for the first time with LModeAGen,
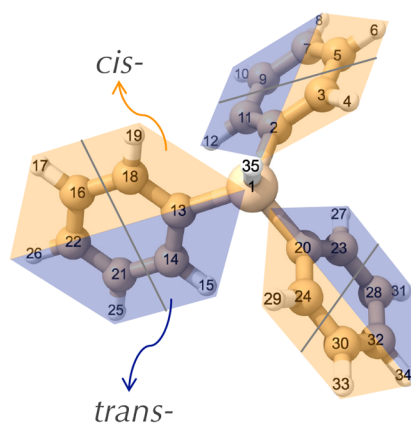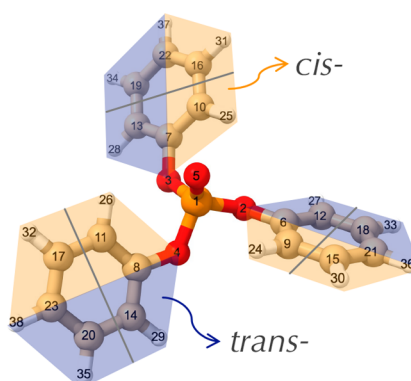
Selected Local Vibrational Modes

ortho- C – H equivalent bonds
ω^a(C3H4)   =   3178 cm^{-1}
ω^a(C18H19)   =   3178 cm^{-1}
ω^a(C24H29)   =   3178 cm^{-1}
ω^a(C11H12)   =   3189 cm^{-1}
ω^a(C14H15)   =   3189 cm^{-1}
ω^a(C23H27)   =   3189 cm^{-1}

meta- C – H equivalent bonds
ω^a(C28H31)   =   3200 cm^{-1}
ω^a(C9H10)   =   3200 cm^{-1}
ω^a(C21H25)   =   3200 cm^{-1}
ω^a(C5H6)   =   3202 cm^{-1}
ω^a(C16H17)   =   3202 cm^{-1}
ω^a(C30H33)   =   3202 cm^{-1}

para- C – H equivalent bonds
ω^a(C7H8)   =   3203 cm^{-1}
ω^a(C22H26)   =   3203 cm^{-1}
ω^a(C32H34)   =   3203 cm^{-1}

(a)

Selected Local Vibrational Modes

meta- C – H equivalent bonds
ω^a(C15H30)   =   3210 cm^{-1}
ω^a(C17H32)   =   3210 cm^{-1}
ω^a(C16H31)   =   3210 cm^{-1}
ω^a(C18H33)   =   3212 cm^{-1}
ω^a(C19H34)   =   3212 cm^{-1}
ω^a(C20H35)   =   3212 cm^{-1}

para- C – H equivalent bonds
ω^a(C21H36)   =   3213 cm^{-1}
ω^a(C22H37)   =   3213 cm^{-1}
ω^a(C23H38)   =   3213 cm^{-1}

ortho- C – H equivalent bonds
ω^a(C12H27)   =   3218 cm^{-1}
ω^a(C13H28)   =   3218 cm^{-1}
ω^a(C14H29)   =   3218 cm^{-1}
ω^a(C9H24)   =   3229 cm^{-1}
ω^a(C11H26)   =   3229 cm^{-1}
ω^a(C10H25)   =   3229 cm^{-1}

(b)

Figure 14. (a) Triphenylsilane and (b) triphenyl phosphate structures with indications of *ortho-*, *meta-*, and *para-*C−H equivalent bonds and their local mode stretching frequencies.

these ACS and CNM procedures for QM/MM systems are now possible.

ACS analyses of test examples **9**−**11** (Figures 17, 18, and 19) reveal that the local mode frequencies below 800 cm^{-1} are composed of LVMs associated with bond stretching vibrations (N−Fe and C−Fe), as well as angular and dihedral distortions (N−Fe−C, O−C−Fe, C−N−Fe, C−C−N−Fe, C−N−Fe−C, N−Fe−C−N), which involve the Fe atom. Test example **9**

(C_{4v} symmetry) has more degenerate LVMs than test examples **10** and **11** (both in the C_1 symmetry), leading to a more condensed ACS plot. Test example **9** has eight degenerate C−C−N−Fe and C−N−Fe−C dihedral angle LVMs (with local mode frequencies at 256 and 272 cm^{-1} in Figure 17), which are quasi-degenerate in test example **10** (Figure 18) and nondegenerate in test example **11** (Figure 19). Similar results are found for all LVMs, which are equivalent by symmetry in
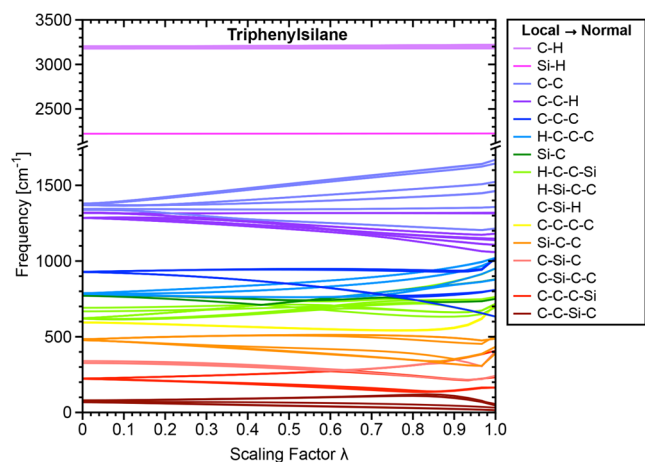
Figure 15. ACS plots of test example **7** (triphenylsilane) relating local mode frequencies (left) with normal-mode frequencies (right). Local vibrational modes are indicated, while normal vibrational mode symmetries are suppressed. ωB97X-D/aug-cc-pVDZ level of theory.
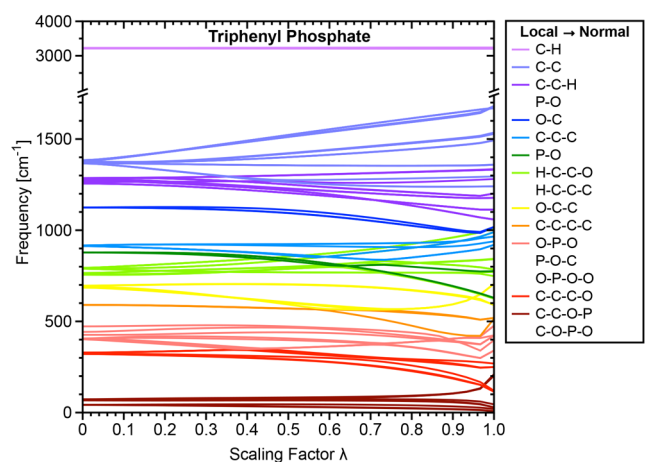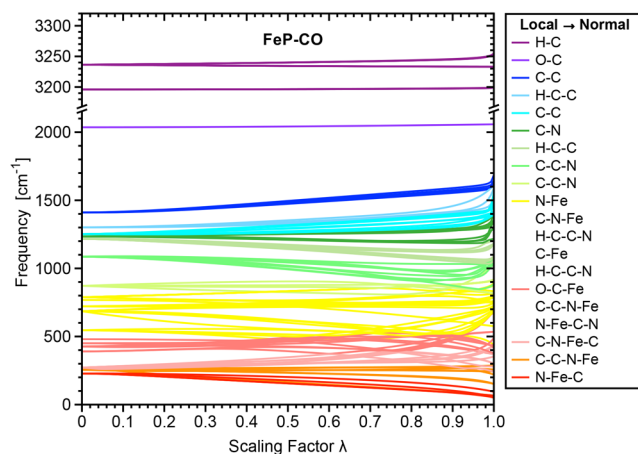

Figure 17. ACS plots of test example **9** (ligated Fe(II)-porphyrin FeP−L, with L = CO) at the M06L/def2-TZVP level of theory relating local mode frequencies (left) with normal-mode frequencies (right). Local vibrational modes are indicated, while normal vibrational mode symmetries are suppressed.

Figure 16. ACS plots of test example **8** (triphenyl phosphate) relating local mode frequencies (left) with normal-mode frequencies (right). Local vibrational modes are indicated, while normal vibrational mode symmetries are suppressed. ωB97X-D/aug-cc-pVDZ level of theory.

Figure 18. ACS plots of test example **10** (ligated Fe(II)-porphyrin L′−FeP−L, with L = CO, L′ = imidazole) at the M06L/def2-TZVP level of theory relating local mode frequencies (left) with normal-mode frequencies (right). Local vibrational modes are indicated, while normal vibrational mode symmetries are suppressed.
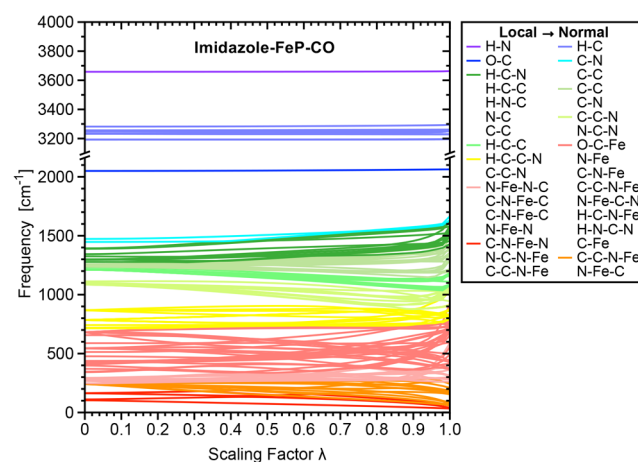
test example **9**, but the equivalence is broken by substituent effects in test examples **10** and **11**. It is noteworthy that LModeAGen, even after analyzing these three system Graphs independently, provides consistent LVM parameters.

LModeAGen analysis of test example **9** leads to the recognition of eight different cyclic type fragments, indicated in Figure 20. As a consequence, eight closing-ring atoms defined one additional bond and one less angle. Figure 20 also depicts selected equivalent LVMs determined by local mode analysis. As examples, eight degenerate C−C−N−Fe dihedral angles appear with a local frequency at 256 cm^{-1}, while eight degenerate Fe−N−C angles have local frequency at 685 cm^{-1}. Three-fold eight degenerate LVMs for C−C bonds were determined by a local mode analysis, with C−C bonds that are closer to the N atoms in the pyrrole rings being the weaker ones. C−H bond stretching LVMs are also degenerate and are separated in two groups: eight C−H stretches belonging to pyrrole rings and four C−H stretches belonging to the C atoms connecting the pyrrole rings, as depicted in Figure 20.

The Fe−C−O moiety in test examples **9** and **10** is linear, which are characterized by our algorithm as linear subsystems.

Bearing resemblance to CO_2 (test example **1**), two-degenerate angles are defined for Fe−C−O. This is avoided by the algorithm for other linear adjacent bonds such as the different moiety of *trans*-N−Fe−N. For test example **9**, these two angle LVMs are found with a local mode frequency at 391 cm^{-1}, while in test example **10** the symmetry is broken and they are quasi-degenerate with local mode frequencies at 342 and 347 cm^{-1}, in which the higher frequency corresponds to the angular distortion along the same plane as that of the imidazole group. In test example **11**, the Fe−C−O moiety is not linear due to the histidine interaction, leading to a set composed of an angle and a dihedral angle LVMs rather than two degenerate angle LVMs. Similar to test example **9**, LModeAGen recognized in test examples **10** and **11**, a total of nine and ten cycles, leading to respective amounts of more bonds and less angles LVMs.

In test examples **9** and **10**, LVMs related to angular (C−C−N, H−C−C, N−C−N, and H−C−N) and dihedral distortions (H−C−C−N and H−C−C−C) appear in the local mode
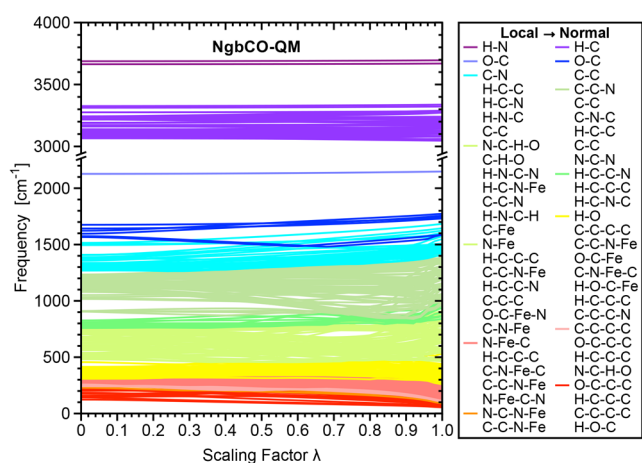
Figure 19. ACS plots of test example **11** (QM subsystem of the active site of carboxy-neuroglobin, NgbCO-QM) at the ωB97X-D/6-31G(d,p)/AMBER level of theory relating local mode frequencies (left) with normal-mode frequencies (right). Local vibrational modes are indicated, while normal vibrational mode symmetries are suppressed.
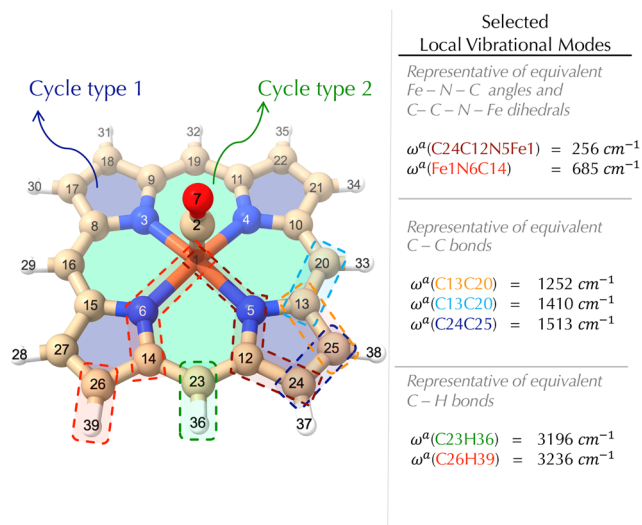

Figure 20. Selected local mode frequencies of test example **9** (ligated Fe(II)-porphyrin FeP-L, with L = CO) with indications of the corresponding parameters in the structure. Cycle types are indicated as well.

frequency range of $720{-}1200$ cm^{-1}, whereas those associated with C−N and C−C bonds, as well as with H−C−C and H−C−N (N at imidazole in test example **11**) angles, appear with local mode frequencies within $1200{-}1470$ cm^{-1}. In system **11**, all of these LVMs are mixed with local mode frequencies in the range of about $750{-}1500$ cm^{-1}, including new LVMs arising from the functional groups in the porphyrin macrocycle local mode frequencies within $1550{-}1675$ cm^{-1}. All C−H bond stretching LVMs in test examples **9**, **10**, and **11** appear with local mode frequencies in the range of $3060{-}3330$ cm^{-1}, while N−H bond LVMs in test examples **10** and **11** appear within $3660{-}3690$ cm^{-1}.

It is expected that $\tilde{\nu}(\text{Fe−C})$ increases and $\tilde{\nu}(\text{C−O})$ decreases when Fe is in an electron-rich coordination environment due to the Fe → CO back-donation effect.[36,71−74] From test example **9** (FeP-CO) to **10** (Imidazole-FeP-CO),

there occurs a decrease in both $k^{\text{a}}_{\text{Fe−C}}$ and $\omega^{\text{a}}_{\text{Fe−C}}$, from 3.43 to 2.51 mDyn/Å and from 768 to 656 cm^{-1}, respectively. Such trend is followed by a slight increase in $k^{\text{a}}_{\text{C−O}}$ and $\omega^{\text{a}}_{\text{C−O}}$ values, from 16.75 to 16.97 mDyn/Å and from 2036 to 2050 cm^{-1}, respectively. From test example **10** (an isolated molecule) to **11** (a system in a protein environment), the differences in the porphyrin functional groups, and different binding in the protein pocket (including proximal imidazole and distal histidine interactions) result in an increase in the Fe−C bond strength. The values of $k^{\text{a}}_{\text{Fe−C}}$ and $\omega^{\text{a}}_{\text{Fe−C}}$ vary from 2.51 to 3.17 mDyn/Å and from 656 to 738 cm^{-1}, respectively, in test example **10** and **11**. An increase in the C−O bond strength is verified as well, with $k^{\text{a}}_{\text{C−O}}$ and $\omega^{\text{a}}_{\text{C−O}}$ going from 16.97 to 18.28 mDyn/Å and from 2050 to 2127 cm^{-1}, respectively. These results are in line with the previous work from our group,[36] where NgbCO in the ϵ tautomeric form of the distal histidine H64ϵ does not form a H-bond with the heme pocket involving the H−N bond, but has a steric repulsion with the histidine ring. As a consequence, a slightly bent Fe−C−O angle ($173.5°$) and a higher C−O bond strength are observed when test example **11** is compared with test example **10**.

N−Fe bond stretching appears with a small contribution in the normal mode with a frequency at 993 cm^{-1}. That normal mode has the following CNM contributions: 44% and 28% for N−C−N and C−C−N angle distortions; 7% for N−Fe bond stretching; 6% and 4% for two nondegenerate C−N−Fe angle distortions. Table 1 (selected results) and Figures S8−S10 (Supporting Information) collect the localized NVMs for test examples **9**−**11**.

■ CONCLUSIONS

ACS and CNM are powerful tools of the local mode theory to decipher electronic structure information encoded in vibrational spectroscopy data, which has already led to a new way of analyzing vibrational spectra.[24] The actual bottleneck for a successful application of the ACS and CNM analysis is the proper choice of a chemically meaningful complete and nonredundant set of local mode parameters, which can become unfeasible for complex systems or systems with a large number of atoms (>100) when performed manually or starting from a huge redundant coordinate set and applying some trial and error procedures. Hence, our new protocol is an important step forward for the routine local mode analysis including ACS and/or CNM for complex and/or large systems with hundreds of atoms. Our work opens the door to reliably obtaining local vibrational mode parameters with an easy-to-use procedure that applies to generic systems with large (>100) number of atoms. The ACS and CNM plots of test examples **1**−**11** give a flavor of the rich information obtained in normal vibrational modes, for example, by shedding new light on the clustering of local vibrational modes in molecular motions of fragments or the change of vibrational modes upon substitution which lowers the symmetry. We hope that this work will inspire the community to use ACS and CNM more frequently as a tool for the analysis of vibrational spectra.

■ ASSOCIATED CONTENT

ⓢ Supporting Information

The Supporting Information is available free of charge at https://pubs.acs.org/doi/10.1021/acs.jpca.2c07871.

QM/MM Methodology for NgbCO Protein; CNM percentage results for selected normal modes (see

Figures S1−S10); molecular geometries (Cartesian coordinates) of test examples **1−11**. LModeAGen and the LModeA package[64] are available upon request. The proper usage of LModeAGen requires an additional input file in *.mol* format[75] from which the molecular Graph will be extracted. All atoms and fragments must be connected (i.e., no isolated fragments can be present in *.mol* file). Files with *.mol* format can be generated using different graphical visualization programs (PDF)

Movies of test examples **1−11** are available in a PowerPoint file (pptx), showing the corresponding movements of the atoms during the NVMs (PPTX)

■ AUTHOR INFORMATION

Corresponding Author

  Elfi Kraka − *Computational and Theoretical Chemistry Group (CATCO), Department of Chemistry, Southern Methodist University, Dallas, Texas 75275-0314, United States;* orcid.org/0000-0002-9658-5626; Email: ekraka@gmail.com

Authors

  Renaldo T.Moura Jr. − *Computational and Theoretical Chemistry Group (CATCO), Department of Chemistry, Southern Methodist University, Dallas, Texas 75275-0314, United States; Department of Chemistry and Physics Center of Agrarian Sciences, Federal University of Paraiba, Areia, PB 58397-000, Brazil*

  Mateus Quintano − *Computational and Theoretical Chemistry Group (CATCO), Department of Chemistry, Southern Methodist University, Dallas, Texas 75275-0314, United States;* orcid.org/0000-0003-4730-0337

  Juliana J. Antonio − *Computational and Theoretical Chemistry Group (CATCO), Department of Chemistry, Southern Methodist University, Dallas, Texas 75275-0314, United States;* orcid.org/0000-0002-0358-9274

  Marek Freindorf − *Computational and Theoretical Chemistry Group (CATCO), Department of Chemistry, Southern Methodist University, Dallas, Texas 75275-0314, United States*

Complete contact information is available at:
https://pubs.acs.org/10.1021/acs.jpca.2c07871

Notes
The authors declare no competing financial interest.

■ ACKNOWLEDGMENTS

■ REFERENCES

(1) Damle, V. H.; Aviv, H.; Tischler, Y. R. Identification of Enantiomers Using Low-Frequency Raman Spectroscopy. *Anal. Chem.* **2022**, *94*, 3188−3193.

(2) Beckmann, R.; Brieuc, F.; Schran, C.; Marx, D. Infrared Spectra at Coupled Cluster Accuracy from Neural Network Representations. *J. Chem. Theory Comput.* **2022**, *18*, 5492−5501.

(3) Cao, Y.; Sun, M. Tip-enhanced Raman spectroscopy. *Rev. Phys.* **2022**, *8*, 100067.

(4) Cozzolino, D. Advantages, Opportunities, and Challenges of Vibrational Spectroscopy as Tool to Monitor Sustainable Food Systems. *Food Anal. Methods* **2022**, *15*, 1390−1396.

(5) Jablonka, K. M.; Patiny, L.; Smit, B. Making Molecules Vibrate: Interactive Web Environment for the Teaching of Infrared Spectroscopy. *J. Chem. Educ.* **2022**, *99*, 561−569.

(6) Manzhos, S.; Ihara, M. Computational vibrational spectroscopy of molecule−surface interactions: what is still difficult and what can be done about it. *Phys. Chem. Chem. Phys.* **2022**, *24*, 15158−15172.

(7) van Adrichem, K. E.; Jansen, T. L. C. AIM: A Mapping Program for Infrared Spectroscopy of Proteins. *J. Chem. Theory Comput.* **2022**, *18*, 3089−3098.

(8) Chaudhary, I.; Jackson, N.; Denning, D.; O'Neill, L.; Byrne, H. J. Contributions of vibrational spectroscopy to virology: A review. *Clin. Spectrosc.* **2022**, *4*, 100022.

(9) Meuwly, M. Atomistic Simulations for Reactions and Vibrational Spectroscopy in the Era of Machine Learning-Quo Vadis? *J. Phys. Chem. B* **2022**, *126*, 2155−2167.

(10) Ditler, E.; Luber, S. Vibrational spectroscopy by means of first-principles molecular dynamics simulations. *WIREs: Comput. Mol. Sci.* **2022**, *12*, No. e1605.

(11) Bērziņš, K.; Fraser-Miller, S. J.; Gordon, K. C. Recent advances in low-frequency Raman spectroscopy for pharmaceutical applications. *Int. J. Pharm.* **2021**, *592*, 120034.

(12) Sawaya, N. P. D.; Paesani, F.; Tabor, D. P. Near- and long-term quantum algorithmic approaches for vibrational spectroscopy. *Phys. Rev. A* **2021**, *104*, 062419.

(13) Beć, K. B.; Grabska, J.; Huck, C. W. Current and future research directions in computer-aided near-infrared spectroscopy: A perspective. *Spectrochim. Acta A Mol. Biomol. Spectrosc.* **2021**, *254*, 119625.

(14) Barone, V.; Alessandrini, S.; Biczysko, M.; Cheeseman, J. R.; Clary, D. C.; McCoy, A. B.; DiRisio, R. J.; Neese, F.; Melosso, M.; Puzzarini, C. Computational molecular spectroscopy. *Nat. Rev. Methods Primers* **2021**, *1*, 38.

(15) Hess, C. New advances in using Raman spectroscopy for the characterization of catalysts and catalytic reactions. *Chem. Soc. Rev.* **2021**, *50*, 3519−3564.

(16) Fick, R. J.; Liu, A. Y.; Nussbaumer, F.; Kreutz, C.; Rangadurai, A.; Xu, Y.; Sommer, R. D.; Shi, H.; Scheiner, S.; Stelling, A. L. Probing the Hydrogen-Bonding Environment of Individual Bases in DNA Duplexes with Isotope-Edited Infrared Spectroscopy. *J. Phys. Chem. B* **2021**, *125*, 7613−7627.

(17) Beć, K. B.; Grabska, J.; Hofer, T. S. In *Near-Infrared Spectroscopy: Theory, Spectral Analysis, Instrumentation, and Applications; Introduction to Quantum Vibrational Spectroscopy*; Ozaki, Y., Huck, C., Tsuchikawa, S., Engelsen, S. B., Eds.; Springer: Singapore, 2021; pp 83−110.

(18) Ozaki, Y.; Beć, K. B.; Morisawa, Y.; Yamamoto, S.; Tanabe, I.; Huck, C. W.; Hofer, T. S. Advances, challenges and perspectives of quantum chemical approaches in molecular spectroscopy of the condensed phase. *Chem. Soc. Rev.* **2021**, *50*, 10917−10954.

(19) Han, X. X.; Rodriguez, R. S.; Haynes, C. L.; Ozaki, Y.; Zhao, B. Surface-enhanced Raman Spectroscopy. *Nat. Rev. Methods Primers* **2021**, *1*, 87.

(20) Orlando, A.; Franceschini, F.; Muscas, C.; Pidkova, S.; Bartoli, M.; Rovere, M.; Tagliaferro, A. A Comprehensive Review on Raman Spectroscopy Applications. *Chemosensors* **2021**, *9*, 262.

(21) Jiang, Y.; Wang, L. Modeling the vibrational couplings of nucleobases. *J. Chem. Phys.* **2020**, *152*, 084114.

(22) Graefe, C. T.; Punihaole, D.; Harris, C. M.; Lynch, M. J.; Leighton, R.; Frontiera, R. R. Far-Field Super-Resolution Vibrational Spectroscopy. *Anal. Chem.* **2019**, *91*, 8723−8731.

(23) Wilson, E. B. Some Mathematical Methods for the Study of Molecular Vibrations. *J. Chem. Phys.* **1941**, *9*, 76−84.

(24) Kraka, E.; Zou, W.; Tao, Y. Decoding Chemical Information from Vibrational Spectroscopy Data: Local Vibrational Mode Theory. *WIREs: Comput. Mol. Sci.* **2020**, *10*, 1480.

(25) Kraka, E.; Quintano, M.; La Force, H. W.; Antonio, J. J.; Freindorf, M. Feature Article: The Local Vibrational Mode Theory and Its Place in the Vibrational Spectroscopy Arena. *J. Phys. Chem. A* **2022**, *126*, 8781.

(26) Konkoli, Z.; Cremer, D. A New Way of Analyzing Vibrational Spectra. I. Derivation of Adiabatic Internal Modes. *Int. J. Quantum Chem.* **1998**, *67*, 1−9.

(27) Konkoli, Z.; Larsson, J. A.; Cremer, D. A New Way of Analyzing Vibrational Spectra. II. Comparison of Internal Mode Frequencies. *Int. J. Quantum Chem.* **1998**, *67*, 11−27.

(28) Konkoli, Z.; Cremer, D. A New Way of Analyzing Vibrational Spectra. III. Characterization of Normal Vibrational Modes in terms of Internal Vibrational Modes. *Int. J. Quantum Chem.* **1998**, *67*, 29−40.

(29) Konkoli, Z.; Larsson, J. A.; Cremer, D. A New Way of Analyzing Vibrational Spectra. IV. Application and Testing of Adiabatic Modes within the Concept of the Characterization of Normal Modes. *Int. J. Quantum Chem.* **1998**, *67*, 41−55.

(30) Cremer, D.; Larsson, J. A.; Kraka, E. In *Theoretical and Computational Chemistry*; Parkanyi, C., Ed.; Elsevier: Amsterdam, 1998; pp 259−327.

(31) Zou, W.; Kalescky, R.; Kraka, E.; Cremer, D. Relating Normal Vibrational Modes to Local Vibrational Modes with the Help of an Adiabatic Connection Scheme. *J. Chem. Phys.* **2012**, *137*, 084114.

(32) Kalescky, R.; Zou, W.; Kraka, E.; Cremer, D. Local Vibrational Modes of the Water Dimer - Comparison of Theory and Experiment. *Chem. Phys. Lett.* **2012**, *554*, 243−247.

(33) Zou, W.; Kalescky, R.; Kraka, E.; Cremer, D. Relating Normal Vibrational Modes to Local Vibrational Modes: Benzene and Naphthalene. *J. Mol. Model.* **2013**, *19*, 2865−2877.

(34) Kalescky, R.; Kraka, E.; Cremer, D. Description of Aromaticity with the Help of Vibrational Spectroscopy: Anthracene and Phenanthrene. *J. Phys. Chem. A* **2014**, *118*, 223−237.

(35) Verma, N.; Tao, Y.; Zou, W.; Chen, X.; Chen, X.; Freindorf, M.; Kraka, E. A Critical Evaluation of Vibrational Stark Effect (VSE) Probes with the Local Vibrational Mode Theory. *Sensors* **2020**, *20*, 2358.

(36) Freindorf, M.; Kraka, E. Critical Assessment of the FeC and CO Bond strength in Carboxymyoglobin - A QM/MM Local Vibrational Mode Study. *J. Mol. Model.* **2020**, *26*, 281.

(37) Yannacone, S.; Freindorf, M.; Tao, Y.; Zou, W.; Kraka, E. Local Vibrational Mode Analysis of π-Hole Interactions between Aryl Donors and Small Molecule Acceptors. *Crystals* **2020**, *10*, 556.

(38) Yannacone, S.; Sayala, K. D.; Freindorf, M.; Tsarevsky, N. V.; Kraka, E. Vibrational Analysis of Benziodoxoles and Benziodazolotetrazoles. *PhysChem* **2021**, *1*, 45−68.

(39) Quintano, M.; Kraka, E. Theoretical insights into the linear relationship between pK_a values and vibrational frequencies. *Chem. Phys. Lett.* **2022**, *803*, 139746.

(40) Randić, M.; Novič, M.; Plavšić, D. *Solved and Unsolved Problems of Structural Chemistry*; CRC Press: Boca Raton, 2016.

(41) Tao, Y.; Tian, C.; Verma, N.; Zou, W.; Wang, C.; Cremer, D.; Kraka, E. Recovering Intrinsic Fragmental Vibrations Using the Generalized Subsystem Vibrational Analysis. *J. Chem. Theory Comput.* **2018**, *14*, 2558−2569.

(42) Tao, Y.; Zou, W.; Nanayakkara, S.; Freindorf, M.; Kraka, E. A revised formulation of the generalized subsystem vibrational analysis (GSVA). *Theor. Chem. Acc.* **2021**, *140*, 31.

(43) Wilson, E. B.; Decius, J. C.; Cross, P. C. *Molecular Vibrations: The Theory of Infrared and Raman Vibrational Spectra*; McGraw-Hill: New York, 1955.

(44) Woodward, L. A. *Introduction to the Theory of Molecular Vibrations and Vibrational Spectroscopy*; Oxford University Press: Oxford, 1972.

(45) Herzberg, G. *Molecular Spectra and Molecular Structure. Vol. II: Infrared and Raman Spectra of Polyatomic Molecules*; Krieger Publishing Co: New York, 1991.

(46) Herzberg, G.; Huber, K. P. *Molecular Spectra and Molecular Structure; IV. Constants of Diatomic Molecules*; Van Nostrand, Reinhold: New York, 1979.

(47) Califano, S. *Vibrational States*; Wiley: New York, 1976.

(48) Zou, W.; Izotov, D.; Cremer, D. New Way of Describing Static and Dynamic Deformations of the Jahn-Teller Type in Ring Molecules. *J. Phys. Chem. A* **2011**, *115*, 8731−8742.

(49) Zou, W.; Filatov, M.; Cremer, D. Bond Pseudorotation, Jahn-Teller, and Pseudo-Jahn-Teller Effects in the Cyclopentadienyl Cation and its Pentahalogeno Derivatives. *Int. J. Quantum Chem.* **2012**, *112*, 3277−3288.

(50) Zou, W.; Cremer, D. Description of Bond Pseudorotation, Bond Pseudolibration, and Ring Pseudoinversion Processes Caused by the Pseudo-Jahn-Teller Effect: Fluoro Derivatives of the Cyclopropane Radical Cation. *Aust. J. Chem.* **2014**, *67*, 435.

(51) Cremer, D.; Pople, J. A. General Definition of Ring Puckering Coordinates. *J. Am. Chem. Soc.* **1975**, *97*, 1354−1358.

(52) Frisch, M. J.; Trucks, G. W.; Schlegel, H. B.; Scuseria, G. E.; Robb, M. A.; Cheeseman, J. R.; Scalmani, G.; Barone, V.; Petersson, G. A.; Nakatsuji, H.; et al. *Gaussian 16*, Revision C.01.; Gaussian Inc.: Wallingford, CT, 2016.

(53) Decius, J. C. Compliance Matrix and Molecular Vibrations. *J. Chem. Phys.* **1963**, *38*, 241−248.

(54) Gräfenstein, J.; Cremer, D. Efficient density-functional theory integrations by locally augmented radial grids. *J. Chem. Phys.* **2007**, *127*, 164113.

(55) Chai, J.-D.; Head-Gordon, M. Long-range corrected hybrid density functionals with damped atom−atom dispersion corrections. *Phys. Chem. Chem. Phys.* **2008**, *10*, 6615−6620.

(56) Kendall, R. A.; Dunning, T. H.; Harrison, R. J. Electron affinities of the first-row atoms revisited. Systematic basis sets and wave functions. *J. Chem. Phys.* **1992**, *96*, 6796−6806.

(57) Dunning, T. H. Gaussian basis sets for use in correlated molecular calculations. I. The atoms boron through neon and hydrogen. *J. Chem. Phys.* **1989**, *90*, 1007−1023.

(58) Wang, Y.; Jin, X.; Yu, H. S.; Truhlar, D. G.; He, X. Revised M06-L functional for improved accuracy on chemical reaction barrier heights, noncovalent interactions, and solid-state physics. *Proc. Natl. Acad. Sci. U.S.A.* **2017**, *114*, 8487−8492.

(59) Weigend, F.; Ahlrichs, R. Balanced basis sets of split valence, triple zeta valence and quadruple zeta valence quality for H to Rn: Design and assessment of accuracy. *Phys. Chem. Chem. Phys.* **2005**, *7*, 3297−3305.

(60) Ditchfield, R.; Hehre, W. J.; Pople, J. A. Self−Consistent Molecular−Orbital Methods. IX. An Extended Gaussian−Type Basis for Molecular−Orbital Studies of Organic Molecules. *J. Chem. Phys.* **1971**, *54*, 724−728.

(61) Case, D. A.; et al. *AMBER*; University of California: San Francisco, 2018.

(62) Chung, L. W.; Sameera, W. M. C.; Ramozzi, R.; Page, A. J.; Hatanaka, M.; Petrova, G. P.; Harris, T. V.; Li, X.; Ke, Z.; Liu, F.; Li, H.-B.; Ding, L.; Morokuma, K. The ONIOM Method and Its Applications. *Chem. Rev.* **2015**, *115*, 5678−5796.

(63) Vallone, B.; Nienhaus, K.; Matthes, A.; Brunori, M.; Nienhaus, G. U. The structure of carbonmonoxy neuroglobin reveals a heme−sliding mechanism for control of ligand affinity. *Proc. Natl. Acad. Sci. U.S.A.* **2004**, *101*, 17351−17356.

(64) Zou, W.; Tao, Y.; Freindorf, M.; Makoś, M. Z.; Verma, N.; Cremer, D.; Kraka, E. *Local Vibrational Mode Analysis (LModeA. Computational and Theoretical Chemistry Group (CATCO))*; Southern Methodist University: Dallas, TX, U.S.A., 2022.

(65) McKean, D. C. Individual CH bond strengths in simple organic compounds: effects of conformation and substitution. *Chem. Soc. Rev.* **1978**, *7*, 399−422.

(66) Tao, Y.; Zou, W.; Cremer, D.; Kraka, E. Characterizing Chemical Similarity with Vibrational Spectroscopy: New Insights into the Substituent Effects in Monosubstituted Benzenes. *J. Phys. Chem. A* **2017**, *121*, 8086−8096.

(67) Hansch, C.; Leo, A.; Taft, R. A survey of Hammett substituent constants and resonance and field parameters. *Chem. Rev.* **1991**, *91*, 165−195.

(68) Fey, N.; Orpen, A. G.; Harvey, J. N. Building ligand knowledge bases for organometallic chemistry: Computational description of phosphorus(III)-donor ligands and the metal−phosphorus bond. *Coord. Chem. Rev.* **2009**, *253*, 704−722.

(69) Sandblom, N.; Ziegler, T.; Chivers, T. A density functional study of the bonding in tertiary phosphine chalcogenides and related molecules. *Can. J. Chem.* **1996**, *74*, 2363−2371.

(70) Freindorf, M.; Delgado, A. A. A.; Kraka, E. CO Bonding in Hexa− and Pentacoordinate Carboxy−Neuroglobin − A QM/MM and Local Vibrational Mode Study. *J. Comput. Chem.* **2022**, *43*, 1725−1746.

(71) Ray, G. B.; Li, X. Y.; Ibers, J. A.; Sessler, J. L.; Spiro, T. G. How far can proteins bend the FeCO unit? Distal polar and steric effects in heme proteins and models. *J. Am. Chem. Soc.* **1994**, *116*, 162−176.

(72) Vogel, K. M.; Kozlowski, P. M.; Zgierski, M. Z.; Spiro, T. G. Determinants of the FeXO (X = C, N, O) Vibrational Frequencies in Heme Adducts from Experiment and Density Functional Theory. *J. Am. Chem. Soc.* **1999**, *121*, 9915−9921.

(73) Giordano, D.; Boron, I.; Abbruzzetti, S.; Van Leuven, W.; Nicoletti, F. P.; Forti, F.; Bruno, S.; Cheng, C. C.; Moens, L.; di Prisco, G.; et al. Biophysical Characterisation of Neuroglobin of the Icefish, a Natural Knockout for Hemoglobin and Myoglobin. Comparison with Human Neuroglobin. *PloS One* **2012**, *7*, No. e44508.

(74) Spiro, T. G.; Soldatova, A. V.; Balakrishnan, G. CO NO and O_2 as Vibrational Probes of Heme Protein Interactions. *Coord. Chem. Rev.* **2013**, *257*, 511−527.

(75) Dalby, A.; Nourse, J. G.; Hounshell, W. D.; Gushurst, A. K. I.; Grier, D. L.; Leland, B. A.; Laufer, J. Description of several chemical structure file formats used by computer programs developed at Molecular Design Limited. *J. Chem. Inf. Comput. Sci.* **1992**, *32*, 244−255.

▢ Recommended by ACS